

# 1 **Combinatorial CRISPR screening reveals functional buffering** 2 **in autophagy**

## 3 4 5 **AUTHORS**

6 Valentina Diehl (1, #), Martin Wegner (1, #), Paolo Grumati (1, 6, #), Koraljka Husnjak (1), Simone  
7 Schaubeck (1), Andrea Gubas (1), Varun Jayeshkumar Shah (1), Felix Langschied (2), Alkmini  
8 Kalousi (1), Ingo Ebersberger (2), Ivan Dikic (1, 3-5, \*), and Manuel Kaulich (1, 3-4, \*)

## 9 10 **AFFILIATIONS**

11 1 - Institute of Biochemistry II, Faculty of Medicine, Goethe University Frankfurt, Theodor-Stern-Kai 7,  
12 60590 Frankfurt am Main, Germany.

13 2 - Applied Bioinformatics Group, Institute of Cell Biology and Neuroscience, Goethe University Frankfurt,  
14 Germany.

15 3 - Frankfurt Cancer Institute, Frankfurt am Main, Germany.

16 4 - Cardio-Pulmonary Institute, Frankfurt am Main, Germany.

17 5 - Buchmann Institute for Molecular Life Sciences, Goethe University Frankfurt, Max-von-Laue-Str. 15,  
18 60438 Frankfurt am Main, Germany.

19 6 - current address: Telethon Institute of Genetics and Medicine, Via Campi Flegrei 34, 80078 Pozzuoli  
20 (NA), Italy

21 # - equal contribution

22 \* - correspondence: Manuel Kaulich, [kaulich@em.uni-frankfurt.de](mailto:kaulich@em.uni-frankfurt.de), and

23 Ivan Dikic, [dikic@biochem2.uni-frankfurt.de](mailto:dikic@biochem2.uni-frankfurt.de)

## 24 **ABSTRACT**

25 Functional genomics studies in model organisms and human cell lines provided important insights  
26 into gene functions and their context-dependent role in genetic circuits. However, our functional  
27 understanding of many of these genes and how they combinatorically regulate key biological  
28 processes, remains limited. To enable the SpCas9-dependent mapping of gene-gene interactions  
29 in human cells, we established 3Cs multiplexing for the generation of combinatorial gRNA libraries  
30 in a distribution-unbiased manner and demonstrate its robust performance. The optimal number  
31 for combinatorial hit calling was 16 gRNA pairs and the skew of a library's distribution was  
32 identified as a critical parameter dictating experimental scale and data quality. Our approach  
33 enabled us to investigate 247,032 gRNA-pairs targeting 12,736 gene-interactions in human  
34 autophagy. We identified novel genes essential for autophagy and provide experimental evidence  
35 that gene-associated categories of phenotypic strengths exist in autophagy. Furthermore, circuits  
36 of autophagy gene interactions reveal redundant nodes driven by paralog genes. Our  
37 combinatorial 3Cs approach is broadly suitable to investigate unexpected gene-interaction  
38 phenotypes in unperturbed and diseased cell contexts.

39

## 40 **INTRODUCTION**

41 Combinatorial gRNA expression (gRNA multiplexing) for related or orthogonal CRISPR  
42 applications enable the comprehensive characterization of genetic interactions in human cells.  
43 Several methods are available to support the generation of combinatorial gRNA expression  
44 systems, 1) restriction enzyme-based<sup>1-4</sup>, 2) golden-gate assembly<sup>5-8</sup>, 3) gateway-dependent<sup>9,10</sup>,  
45 as well as 4) recombination-dependent gRNA cloning techniques<sup>11</sup>. These systems are widely  
46 used to clone gRNA sequences in combination with RNA polymerase III promoters, resulting in  
47 arrayed gRNA-expression cassettes. In contrast, RNA polymerase II promoters generate RNA  
48 transcripts that can contain multiple gRNA sequences, although these transcripts require post-  
49 transcriptional processing to yield functional gRNA sequences and are currently limited to Cas12  
50 applications<sup>12,13</sup>. The most widely used Cas-nuclease thus far is SpCas9, though a cloning-free  
51 gRNA multiplexing concept for Cas9 gRNAs is currently lacking, because repetitive and  
52 homologous sequences are unstable in lentiviral vectors<sup>14-16</sup>, rendering them less suited for large-  
53 scale combinatorial screening.

54 Concomitant mutations in two genes can yield unexpected phenotypes with respect to each  
55 gene's individual phenotype<sup>17</sup>. Synthetic lethality as the most extreme combinatorial phenotype  
56 has clinical applications and is under therapeutic exploration<sup>18-20</sup>. A prominent example of a

57 synthetic lethal gene pair with clinical relevance is poly (ADP-ribose) polymerase (PARP)  
58 inhibition in the context of defective *BRCA1* or *BRCA2* genes<sup>15,21,22</sup>. Additionally to this DNA-  
59 damage repair-related example, synthetic lethal interactions have been identified in combinatorial  
60 gRNA CRISPR screens, including the apoptotic genes *BCL2L1* and *MCL1* or *BCL2L1* and  
61 *BCL2L2*<sup>16,23,24</sup>, the mitogen-activated protein kinases 1 and 3 (*MAPK1* and *MAPK3*)<sup>1</sup>, as well as the  
62 PIP<sub>3</sub> phosphatase *PTEN* and the mammalian target of rapamycin *MTOR*<sup>25,26</sup>. To perform pairwise  
63 hit calling in CRISPR screens, two methods are currently established: 1) a variational Bayes  
64 approach (GEMINI)<sup>27</sup>, and 2) the difference of expected to measured log<sub>2</sub>-fold-changes (dLFC) in  
65 which the expected log<sub>2</sub>-fold-change of a gRNA combination is the sum of the log<sub>2</sub>-fold-changes  
66 of each individual gRNA when partnered with control gRNAs<sup>16,24</sup>. These computational  
67 approaches have been applied to negative CRISPR screens. However, with combinatorial gRNA  
68 CRISPR screens being mostly performed in drop-out conditions, we lack knowledge of their  
69 performance for Cas9-based combinatorial gRNAs in positive or FACS-based phenotypic  
70 enrichment screens.

71 Bulk and selective autophagy are tightly regulated processes that target cellular material for  
72 lysosomal degradation and their misregulation culminates in abnormal cell growth and cell death  
73 with implications in various human diseases<sup>28,29</sup>. Rationally-engineered fluorescent reporter  
74 systems in combination with high-throughput CRISPR screens facilitated the systematic  
75 categorization of genes based on their essentiality in autophagy. As such, the transmembrane  
76 protein 41B, as well as the ubiquitin-activating enzyme UBA6, and the hybrid ubiquitin-conjugating  
77 enzyme/ubiquitin ligase BIRC6 were recently identified as important players in the autophagy  
78 network<sup>30-35</sup>. Despite the mapping of essential genes, CRISPR screens paired with fluorescent  
79 autophagic reporters revealed the stress-dependent regulation of autophagy-related genes<sup>36-38</sup>,  
80 and provided mechanistic insights into the gene specificity in bulk and selective autophagy by  
81 identifying PARKIN regulators and the ANT complex as essential components for mitophagy<sup>39,40</sup>.  
82 In combination with proximity biotinylation-coupled mass spectrometry, CRISPR screens also  
83 contributed to a spatial proteogenomic understanding of PARK2-dependent mitophagy<sup>41</sup>. Thus,  
84 unbiased CRISPR approaches coupled to fluorescent reporters and mass spectrometry are  
85 valuable approaches to identify vulnerabilities in bulk and selective autophagy for the treatment  
86 of neurodegenerative diseases and cancer<sup>42-44</sup>.

87 Here, we add to our previous work and describe the SpCas9-based 3Cs multiplexing technology  
88 for the generation of dual combinatorial (multiplexed) gRNA libraries with diversities of up to  
89 several hundreds of thousands of gRNA combinations<sup>45</sup>. In addition to identifying critical technical  
90 parameters, we generated a combinatorial library targeting the human autophagy network and

91 performed a fluorescent reporter-based FACS enrichment screen to identify hitherto  
92 uncharacterized single genes and gene interactions essential for autophagy. Our 3Cs multiplexing  
93 technology is widely applicable and can serve as a general tool for the identification of context-  
94 dependent gene interactions at any scale.

95

## 96 **RESULTS**

### 97 **3Cs multiplexed Cas9 gRNA libraries**

98 To expand on our 3Cs technology and enable Cas9 gRNA multiplexing, we generated a lentiviral  
99 Cas9-gRNA expression plasmid (pLenti-Multiplex) by placing a human 7SK (h7SK) promoter  
100 upstream of a previously engineered Cas9-tracrRNA followed by a human U6 (hU6) promoter  
101 upstream of a wildtype Cas9-tracrRNA sequence<sup>46,47</sup>. Both gRNA cassettes contain a gRNA  
102 placeholder sequence encoding for I-CeuI or I-SceI restriction enzyme sites, respectively (Figure  
103 1A)<sup>45</sup>. Furthermore, in addition to a puromycin selection cassette, the plasmid contains an f1  
104 bacteriophage origin of replication sequence in sense direction, supporting the CJ236 bacteria  
105 and M13KO7 bacteriophage-dependent generation of dU-containing single stranded (ss) DNA  
106 (Figure 1A, Supp. Figure 1A). In contrast to single gRNA 3Cs reactions, 3Cs multiplexing is  
107 performed in the presence of two gRNA-encoding oligonucleotide pools of which each contains  
108 unique 5' and 3' homology sequences for annealing to the h7SK or hU6 gRNA cassettes, thereby  
109 generating hetero-duplex dU-containing double stranded (ds) DNA that contains all possible  
110 gRNA combinations of the two oligo pools (Figure 1A). A coverage-based electroporation into  
111 *dut/ung*-positive bacteria results in template-strand depletion and combinatorial gRNA-containing  
112 dsDNA. To test this concept, we designed two gRNA-encoding oligo pools each containing 50  
113 gRNA sequences targeting GFP (pool-1) or mCherry (pool-2) and used them to generate a  
114 combinatorial gRNA library, in addition to the respective single gRNA libraries (Figure 1B). Based  
115 on the typical three-band pattern of 3Cs dsDNA<sup>45,48</sup>, we observed similar yields and quality of dU-  
116 containing hetero-duplex dsDNA after applying two pools in a single 3Cs reaction when compared  
117 to either pool alone (Supp. Figure 1A). Digesting the final libraries with I-CeuI and I-SceI enzymes  
118 confirmed the exclusive presence of gRNA-containing plasmids (Figure 1C). Paired-end next-  
119 generation sequencing (NGS) revealed all three libraries to be complete with distribution skews  
120 of 1.56, 1.17, and 1.53 for GFP, mCherry, and GFP+mCherry, respectively (Figure 1D, Supp.  
121 Figure 1B-C). Most importantly, when packaged into lentiviral particles and transduced into GFP  
122 and mCherry-expressing hTERT-RPE1(Cas9) cells, the combinatorial GFP+mCherry library  
123 induced the simultaneous depletion of GFP and mCherry fluorescence while both single libraries



124 selectively depleted either GFP or mCherry fluorescence (Figure 1E). Thus, 3Cs multiplexing  
125 generates tightly distributed combinatorial gRNA libraries that are functional in human cells.

126

### 127 **3Cs multiplexing decouples sequence distribution and diversity**

128 Current combinatorial gRNA libraries contain 9 to 18 gRNA pairs per gene-pair<sup>3,15,24</sup>, thus, a robust  
129 technology must generate large pairwise gRNA diversities without compromising reagent quality.  
130 We therefore investigated whether 3Cs multiplexing, similar to single gRNA 3Cs<sup>45</sup>, would  
131 decouple library quality from library size. To this end, we designed four oligonucleotide pools per  
132 gRNA cassette in which one, two, three, or four nucleotide positions within a non-human-target  
133 (NHT) gRNA sequence were randomized to mimic increasing combinatorial gRNA diversities (1N,  
134 4\*4=16 combinations; 2N, 16\*16=256 combinations; 3N, 64\*64=4,096, 4N, 256\*256=65,536  
135 combinations). NGS confirmed the libraries to be complete and evenly distributed with areas  
136 under the curve (AUC) between 0.59 and 0.69 (Figure 2A, Supp. Figure 2A-B). Notably, we  
137 identified the distribution skew to be very narrow with ranges from 1.1 (1N) to 1.49 (4N), values  
138 mostly unmatched even with single gRNA libraries (Supp. Figure 2A-B). Thus, 3Cs multiplexing  
139 is a highly robust method to generate combinatorial gRNA libraries with large sequence  
140 diversities.

141

### 142 **Library distribution skew influences experimental scale**

143 Higher replicate correlation was computationally demonstrated to correlate with smaller library  
144 distribution skew and higher library representation<sup>49</sup>. Thus, we aimed at experimentally  
145 investigating to what extent a combinatorial gRNA library's distribution skew contributes to hit  
146 calling accuracy by generating combinatorial libraries with artificially distorted gRNA  
147 representations and screening them in different coverages. We selected a panel of 20 genes  
148 equally divided in 10 core essential (CE) and 10 tumor-suppressor genes (TSGs) and designed  
149 4 gRNAs per gene. As internal controls, we choose 80 pre-validated NHT sequences<sup>50,51</sup>. We  
150 designed two 3Cs oligo pools: pool-1 contained CE and TSG-targeting gRNAs for h7SK and hU6  
151 cassettes in equal ratios (2\*80 gRNAs), while pool-2 consisted exclusively of NHT gRNA  
152 sequences in equal ratios for h7SK and hU6 cassettes (2\*80 gRNAs). To generate artificially  
153 distorted library skews, we mixed both pools in equimolar ratios (1:1), and in ratios of increasing  
154 NHT sequence-molarity (1:10 and 1:100) and applied them to 3Cs multiplexing. NGS confirmed  
155 an increased fraction of NHT reads in the 1:10 and 1:100 libraries (Figure 2B, Supp. Figure 2C),  
156 and revealed an AUC value for the 1:1 library of 0.65, while the 1:10 and 1:100 libraries contained  
157 increased AUC values of 0.85 and 0.9, respectively (Figure 2C). Most importantly, library

158 distribution skews increased from 1.2 (1:1) to 2.4 (1:10) and 13.46 (1:100) (Supp. Figure 2D),  
159 demonstrating that final 3Cs library quality is coupled to an oligo pool's distribution.

160 Using these libraries in representations of 20- and 200-fold, we evaluated a total of 153,600  
161 pairwise gRNA-knockouts in human hTERT-RPE1(Cas9) cells in biological replicates. Pairwise  
162 guide and gene-level counts correlated well for individual libraries and biological replicates (gene  
163 level, 20x - 1:1, Pearson  $r = 0.96$ ; 1:10, Pearson  $r = 1$ ; 1:100, Pearson  $r = 0.79-1$ ; 200x - 1:1,  
164 Pearson  $r = 0.91-0.98$ ; 1:10, Pearson  $r = 0.96-0.97$ ; 1:100, Pearson  $r = 0.98-1$ ; Supp. Figure 3A-  
165 B). We next analyzed the difference of  $\log_2$  fold changes ( $\log_2FC$ ) in our screens by means of  
166 separating essential genes from non-targeting controls and computed Cohen's D statistics (quality  
167 score (QS)), a value recently introduced to quantify screen quality<sup>52</sup>. Quality scores for the 1:1  
168 library in both tested coverages were very high with 2.95 and 3.25 for 20- and 200-fold,  
169 respectively (Figure 2D). However, a decline in screen quality appeared when library distribution  
170 skews increased above 2 (1:10 library, 20x - QS: 1.5, 200x - QS: 2.68; 1:100 library, 20x - -0.44,  
171 200x - -1.17; Figure 2D).

172 We next assessed if higher experimental coverage was able to rescue wider library distribution  
173 skews by identifying essential gene pairs with MAGeCK analyses and cut-off filters set to  
174  $FDR \leq 10\%$  and  $\log_2FC < -0.5$ . Strikingly, the number of retrieved gene pairs per library distribution  
175 skew was nearly identical between 20- and 200-fold coverages (Figure 2E), suggesting that  
176 CRISPR libraries with narrow distribution skews can be screened at minimal experimental  
177 coverage without compromising data quality. Furthermore, these analyses also suggest that  
178 higher experimental coverage is likely insufficient to rescue wider library distribution skews.  
179 Therefore, a library's distribution skew is a critical parameter that should be considered when  
180 designing combinatorial CRISPR libraries and screens.

181

## 182 **The optimal number of pairwise gRNAs for statistical gene-interaction calling**

183 The number of gRNAs per gene has a profound impact on statistical hit calling<sup>53,54</sup>, thus we  
184 analyzed the concordance of essential pairwise genes identified across the two experimental  
185 coverages with increasing numbers of pairwise gRNAs. We down-sampled the 1:1 data sets and  
186 generated a series of read count tables containing between 1 and 16 randomly chosen gRNA  
187 pairs for each gene combination and performed MAGeCK analyses with cut-off filters at  
188  $FDR \leq 10\%$  and  $\log_2FC \leq -0.5$ <sup>53,54</sup>. A total of 100 essential gene interactions exist within both  
189 libraries (10\*10 essential genes), and as expected, 16 pairwise gRNAs per gene interaction  
190 consistently retrieved the largest number of statistically significant essential gene interactions  
191 (200x - 70%, 20x - 72%) (Figure 2F). However, performance differences became evident in the

192 down-sampled libraries containing up to 4 pairwise gRNAs with 13% and 20% paired gene  
193 interactions identified, for 200 and 20-fold library representations, respectively (Figure 2F).  
194 Strikingly, the performance increased noticeably in both coverages up until 13 pairwise gRNAs  
195 from which on the performance plateaued (Figure 2F). These results are consistent with previous  
196 observations for single gRNA SpCas9-dependent CRISPR screens, in which 4 to 6 gRNAs per  
197 gene have been identified for robust statistical hit calling<sup>55</sup>. Assuming the generation of gRNA  
198 number-balanced libraries, our observations identify 16 pairwise gRNAs (4\*4) as the optimal  
199 number for statistical gene-interaction calling.

200

### 201 **Single and inherent-single gRNA enrichment screens are complementary**

202 Pairwise gRNA screens have been applied to phenotypes related to cell viability (drop-outs), but  
203 their performance in enrichment-based screens remains elusive. To address this question, we  
204 identified parameters to investigate pairwise gene interactions in the self-degrading process of  
205 human autophagy by LC3-coupled fluorescent-dependent enrichment screening. We used the  
206 established GFP-LC3-RFP reporter construct to generate a monoclonal hTERT-RPE1 reporter  
207 cell line and confirmed reporter functionality by mTOR inhibition (Torin1 treatment) alone and in  
208 combination with the autophagy inhibitor Bafilomycin (Supp. Figure 4A)<sup>56</sup>. Next, we assembled a  
209 literature-curated list of 192 “extended autophagy” genes that included, among others, autophagy-  
210 related genes (ATGs), autophagy receptors, as well as transcription factors and deubiquitinases,  
211 plus 7 core essential genes as negative controls. To generate a combinatorial gRNA library, we  
212 designed a second oligo pool, named “core autophagy”, consisting of 64 commonly considered  
213 core autophagy genes (Figure 3A, core autophagy, Supp. Table 1). For each gene, we designed  
214 4 gRNA sequences using rule set 2 and added 10% NHT sequences to each pool<sup>51</sup>, resulting in  
215 a total of 876 gRNAs in the “extended autophagy” pool and 282 gRNAs in the “core autophagy”  
216 pool, together generating 247,032 pairwise gRNAs (Figure 3A). We applied the extended  
217 autophagy pool alone and in combination with the core autophagy pool to 3Cs reactions and  
218 generated the single gRNA and pairwise gRNA libraries, respectively. NGS revealed narrow  
219 distribution skews (single library, skew ratio=1.22; multiplex library, skew ratio=1.69) and AUC  
220 values of 0.65 and 0.68 (Supp. Figure 4B-D), supporting our previous observation that 3Cs  
221 multiplexing is a highly robust method for the generation of combinatorial gRNA libraries.  
222 To benchmark our screening approach, we first applied the single autophagy library to screen for  
223 genes essential for Torin1-induced autophagy (Figure 3B). In order to reduce the number of false-  
224 positive hits, we chose stringent FACS-gating criteria that only enriched cells in which autophagy  
225 was completely blocked (Figure 3C, single screen). Importantly, proliferative effects as a

226 consequence of gene knockouts are a source of false-positive hit calling in enrichment screens,  
227 especially in TP53-positive cells. Thus, we collected a coverage-based cell sample at the day of  
228 FACS sorting to correct for positive or negative proliferative effects (Figure 3B). Guide RNA and  
229 gene level correlations between pre- and post-FACS samples were high among biological  
230 replicates (guide level, Pearson  $r=0.87$ ; gene level, Pearson  $r=0.97$ ; Supp. Figure 5A-B), thus we  
231 applied MAGeCK and retrieved 12 significantly enriched genes with  $\log_2FC$  between 3.76 and  
232 9.12 with  $FDR \leq 10\%$  (Supp. Table 2). Importantly, our benchmark screen successfully retrieved  
233 previously identified core autophagy genes required for mTOR-induced autophagy and correctly  
234 assigned their function to bulk autophagy by means of a positive  $\log_2FC$  between pre- and post-  
235 FACS conditions (Figure 3D)<sup>32,33,35,39,40,57,58</sup>.

236 Next, we dramatically scaled up to perform the autophagy multiplex screen at a 20-fold coverage  
237 at pre- and post-FACS time points, investigating a total of 1,235,160 pairwise gRNAs. Guide RNA  
238 and gene level correlations between pre- and post-FACS samples were high among biological  
239 triplicates: gRNA level, pre-FACS, Pearson  $r=0.99$ ; post-FACS, Pearson  $r=0.58-0.69$ ; gene level,  
240 pre-FACS, Pearson  $r=0.99$ ; post-FACS, Pearson  $r=0.77-0.84$  (Supp. Figure 5A, C-D). During the  
241 course of FACS sorting, we noticed a population of cells that was absent from single gRNA  
242 transduced cells and extended our sorting strategy to also investigate cells from this “high-gate”  
243 (Figure 3C). We first assessed the nature of the high-gate cell population and identified the  
244 majority of reads to account for ATG4B-dependent gRNA pairs (post-FACS 1, 86.94%; post-  
245 FACS 2, 78.03%; post-FACS 3, 75.53%) (Supp. Figure 5E). To permit its function, ATG4 cleaves  
246 the LC3-reporter and paired ATG4 gene knockouts likely interfere with reporter functionality and  
247 served as additional controls to validate our library and screening strategy<sup>56</sup>.

248 Within the combinatorial gRNA library, four sets of gRNA interactions occur, 1) control with control  
249 (NHT:NHT), 2) extended autophagy with control (gene:NHT), 3) control with core autophagy  
250 (NHT:gene), and 4) extended autophagy with core autophagy (gene:gene) (Figure 3A). Thus, we  
251 next assessed the concordance of identified single genes essential for autophagy induction  
252 between our single autophagy benchmark screen and the extended autophagy gRNAs paired  
253 with control guides in the combinatorial screen. We applied MAGeCK to compare pre- and post-  
254 FACS time points and identified 10 significantly enriched genes with  $\log_2FC$  between 1.53 and  
255 2.75 and  $FDR \leq 10\%$  (Figure 3E). Screen concordance was high with 7 jointly identified genes,  
256 though each experiment successfully identified unique genes essential for bulk autophagy  
257 induction (Figure 3D-E, unique hits in blue-bold). Importantly, the jointly identified genes ATG9A,  
258 RB1CC1, ATG12, ATG7, ATG3, and ATG16L1 as well as the unique hit genes ATG101, ATG10,  
259 ATG13, ATG5, ATG14 and TMEM41B could be successfully validated by targeting each gene

260 with a newly designed single gRNA, for which gRNA performance during the course of validation  
261 was quantified by TIDE analysis (Figure 3F). Screen concordance could be further improved to  
262 11 jointly identified genes by filtering for p-values below 0.05 and simultaneously relaxing the  
263 FDR, although the number of uniquely identified genes per screen increased accordingly to 8 and  
264 7 for dedicated single and inherent single screens, respectively (Supp. Figure 6A-B). This  
265 demonstrates that dedicated single and inherent-single autophagy screens are complementary  
266 and that either one alone was insufficient to identify all true-positive hits.

267

### 268 **Synergistic gene pairs essential for autophagy**

269 Targeting single genes with two gRNAs has been shown to improve knockout rates<sup>59</sup>, we  
270 therefore investigated the consistency of this phenotype within our combinatorial data set. As  
271 expected, we repeatedly observed a higher log<sub>2</sub>FC for combinatorial-gRNA targeted genes  
272 (Supp. Figure 7A), particularly for genes that we identified and validated as essential for  
273 autophagy (Supp. Figure 7B). Next, we assessed pairwise gene interactions essential for  
274 autophagy induction by applying MAGeCK to pre- and post-FACS samples. This identified a total  
275 of 3645 significant gene pairs, of which 187 gene pairs accounted for pairs in which both genes  
276 were jointly or uniquely identified as single essential for autophagy (Figure 4A, D). 3245 gene  
277 pairs accounted for gene pairs in which one or the other gene was identified as being essential  
278 for autophagy (Figure 4B, D), and 213 gene pairs consisted of genes for which neither partner  
279 gene was identified as being essential for autophagy (Figure 4C, D). Interactions between the  
280 majority of identified gene pairs are driven by a single gene that is essential for autophagy and  
281 interactions between non-essential autophagy genes are rare, which is well in agreement with  
282 previous work that mapped genetic interactions in *Saccharomyces cerevisiae*<sup>60</sup>. To corroborate  
283 our findings, we set up arrayed dual gene-targeting validations in which either one gene or both  
284 genes were essential for autophagy induction. As expected, targeting two essential autophagy  
285 genes consistently increased the fraction of cells in which autophagy was blocked (Figure 4E),  
286 and pairing an essential autophagy gene with an autophagy-related but non-essential gene also  
287 increased the fraction of cells in which autophagy was blocked (Figure 4F). Interestingly, among  
288 the non-essential:non-essential hits, we identified ULK1, AMBRA1, WIPI2, and BECN1 in  
289 combinations with control gRNAs, suggesting these genes to be essential for autophagy on their  
290 own, a conclusion supported by the literature<sup>33,57</sup>. They have likely missed our attention in the  
291 single gRNA CRISPR screens due to their relatively mild phenotype compared to the other  
292 autophagy essential genes. Indeed, in arrayed single gRNA validations, the depletion of ULK1  
293 and WIPI2 alone blocked autophagy, although the phenotype was milder when compared to



294 ATG9A depletion that we identified as a strong hit (Figure 4G). This suggests, in the context of  
295 hTERT-RPE1 cells and Torin1-induced autophagy, that gene-associated categories of  
296 phenotypic strengths exist in autophagy. Most interestingly, among others, we identified several  
297 gene pairs capable to block autophagy induction (Figure 4C). We noted several gene pairs in  
298 which one gene is either of the Ras-related protein family (RABs) as well as several pairs that  
299 included ATG2A. Among these interactions we identified ATG2A-ATG2B for which the validation  
300 in arrayed dual-gene knockout conditions confirmed the blockage of autophagy only when both  
301 genes are interfered with, experimentally verifying these genes as functional redundant  
302 homologues (Figure 4G).

303 Four mathematical definitions of genetic interactions have been proposed previously (Product  
304 (MULT), Additive (SUM), Log (LOG), and Min (MIN))<sup>17</sup>. We also included a Max (MAX) definition  
305 and applied all models to identify combinatorial phenotypes that are surprising with respect to  
306 each gene's single phenotype. Genetic interactions are rare<sup>60</sup>, we thus computed the deviation of  
307 observed paired-knockout phenotypes from their expectation (delta log<sub>2</sub>FC,  $\Delta\log_2FC$ ) and  
308 identified the MAX model to fit our combinatorial autophagy data set best (Figure 4H), especially  
309 when only considering genes that we identified to be essential for autophagy for which the  
310 deviation from the expectation is low (Supp. Figure 7C). In total, we identified 3665 genetic  
311 interactions that we filtered by significance ( $p \leq 0.05$ ) and  $\Delta\log_2FC$ s above their single standard  
312 deviation, resulting in a total of 57 (1.6%) high confidence synergistic gene pairs (Figure 4I, yellow  
313 dots, Supp. Table 3). To better depict relations among these gene interactions, we performed a  
314 network analysis and identified 5 network components (1, 36 nodes; 2, 10 nodes; 3, 5 nodes; 4,  
315 3 nodes; and 5, 4 x 2 nodes) (Figure 4J). Most importantly, we identified functional redundancy in  
316 autophagosome assembly (ATG2A/B), phosphatidylinositol phosphorylation (PIK3CA/PI4K2A),  
317 phagosome-lysosome fusion (RAB7A/5A and RAB7B/5A), and selective autophagy (PARK2 with  
318 PLEKHM1 and CALCOCO2, OPTN with PINK1, and PARK7 with FAM134B) (Figure 4J).  
319 Furthermore, we identified DNA Damage-Regulated Autophagy Modulator Protein 1 (DRAM1)-  
320 dependent interactions with mitochondrial PINK1 and PARK2 for which the DRAM1-dependent  
321 induction of autophagy was shown to be dependent on mitochondrial protein synthesis  
322 inhibition<sup>61</sup>. Thus, our identified gene interactions likely resemble functional nodes within the  
323 human autophagy circuit in which redundancy exists and point towards gene paralogs as a critical  
324 factor in generating redundancy in autophagy.

325

## 326 **DISCUSSION**

327 Several technologies are available to generate combinatorial gRNA-containing plasmids and  
328 libraries. They mostly depend on open plasmid DNA and PCR amplified gRNA-encoding  
329 oligonucleotide pools, resulting in cloning-artefacts and sequence biases. Our newly developed  
330 3Cs multiplexing technology functions with single stranded template plasmids and oligonucleotide  
331 pools, thereby circumventing additional and unintended sequence representation dispersions.  
332 Passaging coverage and CRISPR library distribution skew have recently been computationally  
333 predicted to be critical factors for data quality<sup>49</sup>. Indeed, our experimental analysis of combinatorial  
334 libraries with varying distribution skews, applied with different passaging coverages, supports this  
335 prediction and identifies a distribution skew of below 2 as a threshold enabling passaging  
336 coverages below 100-fold. Furthermore, we provide experimental evidence that combinatorial  
337 libraries with distribution skews above 2 should be screened with passaging coverages  $\geq 200$  to  
338 compensate for the library's sequence dispersion. However, rescuing libraries with large  
339 distribution skews ( $\geq 10$ ) by applying high passaging coverage is likely going to fail, as the  
340 sequence dispersion is too big to be compensated for due to sequence underrepresentation at  
341 screen initiation.

342 Combinatorial gRNA screens are more frequently performed to identify gene pairs essential for  
343 cell viability. However, as of today, no combinatorial gRNA screen in combination with pathway-  
344 specific fluorescence reporters has been performed. While the inherent single gRNA phenotypes  
345 appear to be sufficient in the context of cell viability screenings, we show that dedicated and  
346 inherent single gRNA screens are complementary for combinatorial enrichment screens. This is  
347 likely due to the strong enrichment of combinatorial gene phenotypes and the associated  
348 underrepresentation of single-gene effects. However, this can be compensated for by including a  
349 dedicated single gene screen when planning combinatorial enrichment screens. Furthermore, we  
350 note that genes associated with strong phenotypes are sufficiently identified by this approach, but  
351 genes causing milder phenotypes will likely miss attention. This obstacle, however, is  
352 circumvented by carefully examining gene-interactions in the class of phenotype-associated non-  
353 essential gene pairs. Indeed, we demonstrate that AMBRA1, ULK1, WIPI2, and BECN1 are  
354 essential for autophagy, even though both single gRNA screens failed to identify them.

355 Genome-wide or combinatorial CRISPR screens demand large numbers of cells. Thus, current  
356 efforts aim at minimizing cell culture demands by providing combinatorial-gRNA minimized  
357 CRISPR libraries<sup>59,62</sup>. Supporting this notion, we identify log<sub>2</sub>FC of dual-gRNA targeted genes to  
358 be larger than their single-gRNA targeted counterpart. Interestingly, this observation was limited  
359 to genes that we identified to be essential for autophagy, supporting the notion that dual-gRNA



360 gene targeting also induces stronger phenotypes in enrichment screens and that minimized  
361 libraries will also be beneficial for these applications.

362 Functional buffering by paralogs has recently been shown to be largely absent from single gRNA  
363 CRISPR screens<sup>63</sup>, suggesting paralogs to contribute to network redundancy. Indeed, we identify  
364 paralogs as functional buffers in autophagy acting in autophagosome assembly (ATG2A/B),  
365 phosphatidylinositol phosphorylation (PIK3CA/PI4K2A), and phagosome-lysosome fusion  
366 (RAB7A/5A and RAB7B/5A). This is profoundly important when therapeutically targeting  
367 autophagy induction in cells that are dependent on high basal autophagy levels such as acute  
368 myeloid leukemia (AML) cells<sup>64</sup>. Lastly, we note that our analysis failed to identify functional  
369 buffering within the mammalian ATG8 family of proteins (LC3s and GABARAPs), as well as within  
370 the protein class of autophagy receptors (FUNDC1, SQSTM1, OPTN, PLEKHM1, PEX13,  
371 CALCOCO2, FAM134B). Furthermore, the lack of buffering gene interactions between ATG8s  
372 and autophagy receptor proteins, together, supports the notion of their cargo selectivity that  
373 prevents these genes to contribute to autophagy redundancy<sup>65</sup>.

374

## 375 **MATERIAL AND METHODS**

### 376 **3Cs multiplex template plasmid DNA and cloning**

377 pLentiCRISPRv2 (Addgene: 98290) was enzymatically digested with AelI and BsiWI and gel  
378 purified to remove the hU6 gRNA- and SpCas9-expressing cassettes. Likewise, the combinatorial  
379 gRNA-expressing cassette of pKLV2.2 (Addgene: 72666) was digested with AelI and BsiWI. The  
380 2030 bp fragment that encodes the combinatorial gRNA-expressing cassettes and a PGK  
381 promoter was gel purified and cloned into the reduced, purified backbone of pLentiCRISPRv2. In  
382 order to generate unique annealing homology for the 3Cs oligonucleotides and enable template  
383 plasmid removal, the h7SK promoter-associated tracrRNA was replaced by a previously  
384 engineered tracrRNA sequence (tracrRNA v2) and h7SK and hU6 promoter-associated gRNA  
385 cloning sites were modified to contain placeholder sequences encoding for I-CeuI and I-SceI  
386 homing endonuclease restriction sites, respectively<sup>66</sup>.

387

### 388 **3Cs oligonucleotide design rules**

389 All oligonucleotides that were used for multiplexed 3Cs gRNA library generation are listed in 'DNA  
390 oligonucleotides'. DNA oligonucleotides were purchased from Sigma-Aldrich, from Integrated  
391 DNA Technologies (IDT) as single or pooled oligonucleotides in o-pool formats, and from Twist  
392 Bioscience as oligonucleotide pools.

393 To discriminate between h7SK and hU6 and enable exclusive annealing to only one expression  
394 cassette, the 3Cs oligonucleotides were designed with two specific homology regions flanking the  
395 intended 20-nt gRNA sequence for either the h7SK or hU6 expression cassettes. The 3Cs h7SK-  
396 oligonucleotides were 57 nts in length ( $T_m$  above 50°C) and matched the 3' end of the h7SK  
397 promoter region and the 5' start of the tracrRNA v2, while the 3Cs hU6-oligonucleotides were 59  
398 nts in length ( $T_m$  above 50°C) and matched the 3' end of the hU6 promoter region and the 5' start  
399 of the tracrRNA v1 in the template plasmids.

400

#### 401 **Generation of sequence distorted 3Cs libraries**

402 For the generation of biased multiplex 3Cs gRNA libraries, two 3Cs oligonucleotide pools were  
403 designed for each expression cassette of the 3Cs multiplex template plasmid following the 3Cs  
404 oligonucleotide design rules. The first pool was composed of tumor suppressor and essential  
405 gene-targeting gRNAs (target pool), while the second pool only included non-human targeting  
406 gRNAs (control pool). To generate three different libraries that represent libraries of different  
407 quality regarding their distribution, the two oligonucleotide pools were mixed in a different ratio for  
408 each of the three libraries. For the first library, the target and control pool were mixed in a 1:1  
409 ratio, to resemble an evenly distributed gRNA library. For the second library a 1:10 ratio of target  
410 to control pool was applied. The third library was generated with a 1:100 ratio, to resemble a  
411 library with highly underrepresented gRNA sequences. The mixed oligonucleotide pools were  
412 phosphorylated, annealed to purified dU-ssDNA of the 3Cs multiplex template plasmid, and the  
413 3CS synthesis reactions were performed as described above.

414

#### 415 **Generation of multiplexed 3Cs- gRNA libraries**

##### 416 *1. Equipment*

417 Desktop microcentrifuge, shaking incubator at 37°C, 1.5 ml collection tubes, filtered sterile pipette  
418 tips, thermoblocks at 90°C and 50°C (e.g., Thermo Fisher, 88870004), an ultracentrifuge capable  
419 of spinning 50 ml falcon tubes at 10,000 rpm (Beckman Coulter Avanti J-30 I ultracentrifuge and  
420 a Beckman JA-12 fixed angle rotor), falcon tubes (polypropylene, 50 ml (Corning 352070)), a Bio-  
421 Rad Gene Pulser electroporation system (BioRad 164–2076), electroporation cuvettes Plus (2  
422 mm, Model no. 620 (BTX)), a gel electrophoresis chamber, erlenmeyer flasks (glass, 200 ml and  
423 500 ml), 10 cm dishes 10 cm plastic culture dishes (Corning, CLS430591), 14 ml round-bottom  
424 polystyrene tubes (e.g. Thermo Fisher, 10568531).

425

##### 426 *2. dU-ssDNA template amplification*

427 *KCM transformation*

428 KCM competent bacteria (*Escherichia coli* strain K12 CJ236, NEB, E4141) were transformed with  
429 3Cs multiplex template plasmid template by mixing 100 ng of DNA with 2  $\mu$ l of 5x KCM buffer  
430 (0.5M KCl, 0.15M CaCl<sub>2</sub>, 0.25M MgCl<sub>2</sub>) and water in a 10  $\mu$ l reaction. After 10 min of incubation  
431 on ice, an equal volume of CJ236 bacteria was added to the DNA/KCM mixture, gently mixed,  
432 and chilled on ice for 15 min. The bacteria–DNA mixture was then incubated at room temperature  
433 for 10 min and subsequently inoculated into 200  $\mu$ l of prewarmed SOC media (ThermoFisher  
434 Scientific, 15544034). Bacteria were incubated at 37°C and 200 rpm for 1 hr and then streaked  
435 on LB-agar plates with ampicillin (100  $\mu$ g/ml) and chloramphenicol (34  $\mu$ g/ml) for incubation  
436 overnight at 37°C.

437

438 *Phage amplification and ssDNA purification*

439 The morning after transformation, a single colony of transformed *E. coli* CJ236 was picked into 1  
440 ml of 2YT media (Roth, 6676.2) supplemented with M13KO7 helper phage (NEB, N0315) to a  
441 final concentration of  $1 \times 10^8$  pfu/ml and ampicillin (final concentration 100  $\mu$ g/ml) to maintain the  
442 host F' episome and the phagemid, respectively. After 2 hrs of shaking at 200 rpm and 37°C,  
443 kanamycin (Roth, T832.3) was added to a final concentration of 25  $\mu$ g/ml to select for bacteria  
444 that have been infected with M13KO7 helper phage. Bacteria were kept at 200 rpm and 37°C for  
445 6 to 8 hrs. Afterwards, the culture was transferred to 30 ml of 2YT media supplemented with  
446 ampicillin (final concentration 100  $\mu$ g/ml) and kanamycin (final concentration 25  $\mu$ g/ml). After an  
447 additional 20 hrs of shaking at 200 rpm and 37°C, the bacterial culture was centrifuged for 10 min  
448 at 10,000 rpm and 4°C in a Beckman JA-12 fixed angle rotor. The supernatant was subsequently  
449 transferred to 6 ml (1/5 of culture volume) PEG/NaCl (20% polyethylene glycol 8,000, 2.5 M NaCl)  
450 and incubated for 1 hr at room temperature to precipitate phage particles. After 10 min of  
451 centrifugation at 10,000 rpm and 4°C in a Beckman JA-12 fixed angle rotor, the phage pellet was  
452 resuspended in 1.5 ml Dulbecco's phosphate-buffered saline (PBS, Sigma, D8662) and  
453 centrifuged at 13,000 rpm for 5 min, before the phage-containing supernatant was transferred to  
454 a clean 1.5 ml microcentrifuge tube and stored at 4°C. Circular ssDNA was purified from the  
455 resuspended phages with the E.Z.N.A. M13 DNA Mini Kit (Omega Bio-Tek, D69001-01) according  
456 to the manufacturer's protocol. Purity of the isolated ssDNA was ensured by agarose gel  
457 electrophoresis and purified ssDNA was stored at 4°C.

458

459 3. *Multiplexed 3Cs-DNA synthesis*

460 The protocol for multiplexed 3Cs-DNA synthesis was adapted from Wegner et al., 2019 and  
461 optimized for reactions on the 3Cs multiplex template plasmid with two specific annealing sites.  
462 The oligonucleotides that were used for 3Cs reactions and the suppliers are listed separately (see  
463 '3Cs oligonucleotide design rules' and 'DNA oligonucleotides').

464  
465 *Oligonucleotide phosphorylation and annealing*  
466 600 ng of oligonucleotides per annealing site (both, 3Cs h7SK- and hU6-oligonucleotides) were  
467 phosphorylated in two separate 20 µl reactions by mixing them with 2 µl 10x TM buffer (0.1 M  
468 MgCl<sub>2</sub>, 0.5 M Tris-HCl, pH 7.5), 2 µl 10 mM ATP (NEB, 0756), 1 µl 100 mM DTT (Cell Signaling  
469 Technology Europe, 7016), 20 units of T4 polynucleotide kinase (NEB, M0201) and water to a  
470 total volume of 20 µl. The mixture was incubated for 1 hr at 37°C. Phosphorylated oligonucleotides  
471 were immediately annealed to purified multiplex dU-ssDNA template by adding both 20 µl  
472 phosphorylation products to 25 µl 10x TM buffer, 20 µg of dU-ssDNA template and water to a total  
473 volume of 250 µl. The mixture was denatured for 5 min at 95°C, annealed for 5 min at 55°C and  
474 cooled down for 10 min at room temperature.

475  
476 *Multiplexed 3Cs-DNA reaction*  
477 3Cs-DNA was generated by adding 10 µl of 10 mM ATP, 10 µl of 100 mM dNTP mix (Roth,  
478 0178.1/2), 15 µl of 100 mM DTT, 2000 ligation units of T4 DNA ligase (NEB, M0202), and 30 units  
479 of T7 DNA polymerase (NEB, M0274) to the annealed oligonucleotide-ssDNA mixture. The 3Cs  
480 synthesis mix was incubated for 12 hrs (overnight) at room temperature. Afterwards the 3Cs  
481 synthesis product was purified and desalted using a GeneJET Gel Extraction Kit (Thermo Fisher,  
482 K0692) according to the following protocol: 600 µl of binding buffer and 5 µl 3M sodium acetate  
483 (Sigma-Aldrich, 71196) were added to the synthesis product, mixed and applied to two purification  
484 columns, which were centrifuged for 3 min at 460 g. The flow-through was applied a second time  
485 to the same purification column to maximize yield. After two wash steps and 3 min of centrifugation  
486 at maximum speed, the DNA was eluted in 50 µl prewarmed water. The 3Cs reaction product was  
487 analyzed by gel electrophoresis alongside the dU-ssDNA template on a 0.8% TAE/agarose gel  
488 (100 V, 30 min).

489  
490 *4. Multiplexed 3Cs-DNA library amplification, clean-up and quality control*

491 *Electroporation of 3Cs synthesis product*

492 To amplify the multiplex 3Cs libraries, the 3Cs-DNA synthesis product was electroporated. To do  
493 so, 400 µl of electrocompetent E. coli (10-beta, NEB, C3020K) were thawed on ice and mixed

494 with 6 µg of purified 3Cs-DNA. For electroporation, the DNA must be eluted in water or a low salt  
495 solution. After that, the mixture was incubated on ice for 15 min and then transferred into a cold  
496 2 mm cuvette (BTX, 45–0125) that was then inserted into a Bio-Rad Gene Pulser with the  
497 following settings: resistance 200 Ω, capacity 25 F, voltage 2.5 kV. After electroporation, cells  
498 were rescued in 25 ml of pre-warmed SOC media and incubated for 30 min at 37°C and 200 rpm.  
499 After 30 min the culture was transferred into 400 ml of LB media supplemented with 100 µg/ml  
500 ampicillin.

501

#### 502 *Determination of transformation efficiency*

503 To ensure library representation during and after amplification, the number of transformants was  
504 determined. After 30 min of incubation at 37°C and 200 rpm subsequently to the electroporation,  
505 a series of 10-fold dilutions of the 10 µl of bacterial culture in sterile Dulbecco's phosphate-  
506 buffered saline (PBS, Sigma, D8662) was prepared. Dilutions were plated in triplicates on LB-  
507 agar containing 100 µg/ml ampicillin and incubated overnight at 37 °C. The next morning, the  
508 obtained colonies were counted. The number of transformants must be at least 100-fold higher  
509 than the library complexity to ensure maintenance of library diversity.

510

#### 511 *I-CeuI and I-SceI clean-up and quality control*

512 Plasmid DNA of overnight liquid cultures was purified using the Qiagen Plasmid Maxi Kit (Qiagen,  
513 12163), according to the manufacturer's protocol to obtain the pre-library (P1). For removal of  
514 residual 3Cs template plasmid from the multiplex pre-library, 3 µg of purified DNA was digested  
515 with 10 units I-SceI (NEB, R0694), 10 units I-CeuI (NEB, R0699) and 5 µl NEB CutSmart buffer  
516 (NEB, B7204) in a reaction volume of 50 µl for 3 hrs at 37°C. After 3 hrs, an additional 10 units of  
517 I-SceI and I-CeuI and 5 µl NEB CutSmart buffer were added, as well as water to a final volume  
518 of 100 µl. After further incubation for additional 3 hours, the digestion reaction was subjected to  
519 gel electrophoresis on a 0.8% TAE/agarose gel (125 V, 40 min) to separate undigested 3Cs  
520 synthesis product from linearized template plasmid. The band resembling the undigested correct  
521 3Cs synthesis product was purified using a Thermo Fisher Scientific GeneJET Gel Extraction Kit,  
522 according to the manufacturer's protocol. Then, the purified 3Cs synthesis product was  
523 electroporated, according to the electroporation protocol described above. The next day, the  
524 resulting final 3Cs multiplex library preparation (P2) was purified from liquid culture using a Qiagen  
525 Plasmid Maxi Kit, according to the manufacturer's protocol and quality controlled by analytical  
526 restriction enzyme digests, SANGER sequencing and by Next Generation Sequencing.

527

## 528 **Next-generation sequencing (NGS)**

### 529 *NGS sample preparation of 3Cs multiplex plasmid libraries*

530 3Cs multiplex plasmid libraries were prepared for NGS as follows: 250 ng of plasmid DNA was  
531 used per PCR reaction and used in a volume of 50  $\mu$ l using Next High-Fidelity 2x PCR Master  
532 Mix (NEB, M0541) (according to the manufacturer's protocol), containing 2.5  $\mu$ l of 10  $\mu$ M primers  
533 each of forward and reverse primers. Depending on the library complexity up to four 50  $\mu$ l  
534 reactions were performed. Primer sequences are listed separately (see 'DNA oligonucleotides').  
535 Thermal cycler parameters were set as follows: initial denaturation at 98°C for 5 min, 15 cycles of  
536 denaturation at 98°C for 30 s, annealing at 65°C for 30 s, extension at 72°C for 40 s, and final  
537 extension at 72°C for 5 min. PCR products were purified from a 1.5 % TAE/agarose gel using a  
538 GeneJet Gel Extraction Kit (Thermo Fisher Scientific), according to manufacturer's protocol.  
539 Purified PCR products were denatured and diluted according to Illumina the guide lines and set  
540 to a final concentration of 2.6 pM in a total volume of 2.2 ml and 15% PhiX control and loaded  
541 onto a MiSeq, NextSeq 500 or NovaSeq sequencer (Illumina), according to manufacturer's  
542 protocol. Sequencing was performed with single- or paired-end reads, 75 or 150 cycles, plus 8  
543 cycles of index reading.

544

### 545 *NGS sample preparation of 3Cs multiplex screening samples*

546 To prepare 3Cs multiplex screening samples, the required amount of genomic DNA for sufficient  
547 coverage was calculated first: for the autophagy single and multiplex FACS screening samples,  
548 the required genomic DNA was calculated as *number of FACS sorted cells*  $\times$   
549 *screening coverage*  $\times$  6.6 pg. For the autophagy multiplex proliferation control screen, the  
550 required genomic DNA was determined by calculating *library complexity*  $\times$   
551 *screening coverage*  $\times$  6.6 pg.

552 The NGS sample preparation of all samples from screening with the biased libraries was  
553 performed with *library complexity*  $\times$  200 (*maximum screening coverage*)  $\times$  6.6 pg DNA. The  
554 calculated amount of genomic DNA was used in a first PCR (PCR1) reaction with 2 to 4  $\mu$ g of  
555 genomic DNA in a 50  $\mu$ l reaction using the Next High-Fidelity 2x PCR Master Mix (NEB, M0541)  
556 (according to the manufacturer's protocol) and 2.5  $\mu$ l of 10  $\mu$ M PCR1 primers, each of forward  
557 and reverse. Thermal cycler parameters were set as follows: initial denaturation at 98°C for 5 min,  
558 15 cycles of denaturation at 98°C for 55 s, annealing at 65°C for 55 s, extension at 72°C for 110  
559 s, and final extension at 72°C for 7 min. After PCR 1, 25  $\mu$ l of PCR 1 product was transferred to  
560 a second PCR reaction (PCR2) in a 100  $\mu$ l reaction with 50  $\mu$ l High-Fidelity 2x PCR Master Mix  
561 and 2.5  $\mu$ l of 10  $\mu$ M PCR 2 primers that contain Illumina adaptors. Primer sequences for PCR1



562 and PCR2 are listed separately (see 'DNA oligonucleotides'). Thermal cycler parameters were  
563 set as follows: initial denaturation at 98°C for 5 min, 10 cycles of denaturation at 98°C for 30 s,  
564 annealing at 65°C for 30 s, extension at 72°C for 40 s, and final extension at 72°C for 5 min. PCR  
565 products were purified from a 1.5 % TAE/agarose gel and processed for NGS sequencing as  
566 described for plasmid libraries.

567

### 568 **NGS data quality control and read count table generation**

569 Raw next generation sequencing data were processed and demultiplexed with bcl2fastq  
570 v2.19.1.403 (Illumina). Read counts of individual gRNAs and gRNA combinations were  
571 determined using cutadapt 2.8, Bowtie2 2.3.0, and custom Python 3 scripts<sup>67,68</sup>. In brief, reads  
572 were trimmed with cutadapt using 5' adapter sequences, truncated to 20 nucleotides, and aligned  
573 to the respective gRNA library using Bowtie2 with no mismatches allowed. The uniformity of each  
574 library distribution was assessed by plotting the cumulative distribution of all sequencing reads as  
575 a Lorenz curve and determining the area under the curve. The library distribution skew (skew  
576 ratio) of each library was determined by plotting the density of read counts and dividing the top  
577 10 quantiles by the bottom 10 quantile. Cohen's D statistics were applied to assess the quality of  
578 the biased libraries by comparing the distributions of non-targeting sequences and sequences  
579 targeting core essential genes<sup>52</sup>. Pairwise sample correlations were determined with Pearson's  
580 correlation of the normalized read counts and visualized with hierarchically clustered heat maps  
581 (Seaborn library 0.10.1)<sup>69</sup>.

582

### 583 **Enrichment analyses**

584 All enrichment analyses using MAGeCK were performed with median normalization of read  
585 counts and gRNAs with zero counts in the control samples were removed. Down-sampling of the  
586 1:1 dataset was performed by randomly choosing 1 to 16 gRNA combinations per gene  
587 combination without replacement followed by individual MAGeCK analyses. gRNA combinations  
588 with an  $FDR \leq 10\%$  and  $\log_2FC \leq -0.5$  were counted as statistically significant hits.

589

### 590 **Genetic interaction models**

591 Interactions of gene pairs were computed according to five different models: SUM, MIN, LOG,  
592 MULT were used according to their definition in<sup>17</sup>, the MAX model defines the expected phenotype  
593 of a double gene-knockout as the maximal phenotype of the individual single gene-knockouts.  
594 The expected phenotypes of all double gene-knockouts were computed based on the phenotype  
595 of the respective single gene knockouts which were defined as the median  $\log_2FC$  (as provided



596 by the MAGeCK analysis output) of all combinations of NHTs and gRNAs targeting the respective  
597 gene. For each model, the deviation of observed paired-knockout phenotypes from their  
598 expectation were expressed as their difference:  $\Delta\log_2FC = \text{observed} - \text{expected}$ . Assuming that  
599 genetic interactions were rare, density plots of the dLFCs for each model were used to identify  
600 the model with the highest number of neutral interactions, indicated by a single large peak around  
601 0 on the x-axis. Using the MAX model, we kept only combinations with  $p \leq 0.05$  and a  $\Delta\log_2FC$   
602 larger than the standard deviation of all  $\Delta\log_2FC$ s.

603

#### 604 **Autophagy gene interaction network**

605 To generate a network visualization based on our derived gene-gene interactions in autophagy,  
606 we exported MAX model-dependent delta  $\log_2FC$  per gene-gene interaction and imported them  
607 into the open source software platform for visualizing complex networks, Cytoscape (3.8.0)<sup>70</sup>. The  
608 style of the derived network was manually curated with the layout being set to a circular one.

609

#### 610 **Cell culture**

611 Cell culture was performed as described previously<sup>45</sup>. In brief, HEK293T cells (ATCC, CRL-3216)  
612 were maintained in Dulbecco's Modified Eagle's Medium (DMEM, Thermo Fisher Scientific,  
613 41965–039) and puromycin-sensitive hTERT–RPE1 cells (provided by Andrew Holland) in  
614 DMEM: Nutrient Mixture F-12 (DMEM/F12, Thermo Fisher Scientific, 11320–074), each  
615 supplemented with 10% fetal bovine serum (FBS, Thermo Fisher Scientific, 10270) and 1%  
616 penicillin-streptomycin (Sigma-Aldrich, P4333) at 37°C with 5% CO<sub>2</sub>. In addition, hTERT–RPE1  
617 cells were supplemented with 0.01 mg/ml hygromycin B (Capricorn Scientific, HYG-H). No  
618 method to ensure the state of authentication has been applied. Mycoplasma contamination testing  
619 was performed immediately after the arrival of the cells and multiple times during the course of  
620 the experiments. The hTERT-RPE1 GFP-LC3-RFP reporter cell line was generated by  
621 transducing hTERT-RPE1(Cas9) cells with retroviral particles generated with the transfer plasmid  
622 pMRX-IP-GFP-LC3-RFP (Addgene: 84573). Single cell clones were isolated and reporter  
623 functionality was tested by Torin1 and Bafilomycin A1 treatments.

624

#### 625 **Genomic DNA extraction**

626 Genomic DNA of cells was purified by resuspending PBS washed pellets of 40-50 million cells in  
627 12 ml of TEX buffer (10 mM Tris-HCl, pH 7.5, 1 mM EDTA, pH 7.9, 0.5% SDS). Then 300  $\mu$ l of  
628 proteinase K (10 mg/m) and 300  $\mu$ l of Ribonuclease A (90 U/mg, 20 mg/ml) were added to the  
629 resuspended cells. The tubes were incubated overnight at 37°C at constant shaking. After

630 complete cell lysis, 4 ml of 5 M NaCl was added, the solution was mixed and incubated at 4 °C  
631 for 40 min. After that the tubes were centrifuged at 14,000xg for 1 hr. The supernatant was  
632 transferred to a fresh tube and 24 ml of ice-cold 96% ethanol was added before the mixture was  
633 placed at -20°C overnight. The next day, the tubes were centrifuged at 14,000xg for 1 hr.  
634 Afterwards the supernatant was removed and the precipitated DNA was washed with ice-cold  
635 70% ethanol. After further centrifugation 14,000xg for 1 hr the supernatant was removed and the  
636 DNA pellet was dried at room temperature and then dissolved in 5 ml of sterile water.

637

### 638 **GFP and mCherry knockouts**

639 To examine the expression of gRNAs from both expression cassettes of the 3Cs multiplex  
640 template plasmid, two oligonucleotide pools were designed following the 3Cs oligonucleotide  
641 design rules. One oligonucleotide pool was designed for the h7SK cassette with 50 gRNAs  
642 targeting eGFP, the second pool was designed for the hU6 expression cassette with 50 gRNA  
643 targeting the mCherry gene. The two pools were used to generate three 3Cs libraries to selectively  
644 target either eGFP (GFP single library) or mCherry (mCherry single library) or both simultaneously  
645 (eGFP-mCherry multiplex library) following the protocol for generation of multiplexed 3Cs- gRNA  
646 libraries described above. Lentiviral supernatant of the three libraries was generated. Monoclonal  
647 hTERT–RPE1 cells with stable SpCas9, eGFP and mCherry expression were plated at 40%  
648 confluency. The next day, the cells were transduced with viral supernatant of one of the three  
649 libraries. After 48 hrs of transduction, cells were selected with puromycin (2.5µM) for 10 days.  
650 Then, eGFP and mCherry ratios were quantified by FACS analysis.

651

### 652 **Generation, quantification and transduction of lentiviral particles**

653 Generation, quantification and transduction of lentiviral particles was performed as described  
654 previously<sup>45</sup>. In brief, the day before transfection, HEK293T cells were seeded to  $2.5 \times 10^5$   
655 cells/ml. To transfect HEK293T cells, transfection media containing 1/10 of culture volume Opti-  
656 MEM I (Thermo Fisher Scientific, 31985–047), 10.5 µl Lipofectamin 2000 (Thermo Fisher  
657 Scientific, 11668019), 1.65 µg/ml transfer vector, 1.35 µg/ml pPAX2 (Addgene: 12260) and 0.5/ml  
658 µg pMD2.G (Addgene: 12259) was prepared. The mixture was incubated for 30 min at room  
659 temperature and added dropwise to the media. Lentiviral supernatant was harvested 48 hr after  
660 transfection and stored at -80°C.

661 To determine the lentiviral titer, hTERT–RPE1 cells were plated in a 6-well plate with 50,000 cells  
662 per well. The following day, cells were transduced in the presence of 8 µg/ml polybrene (Sigma,

663 H9268) and a series of 0.5, 1, 5, and 10  $\mu$ l of viral supernatant. After 2 days of incubation at 37°C,  
664 cells were subjected to puromycin selection for a total duration of 2 weeks, after which established  
665 colonies were counted per viral dilution. The number of colonies in the highest dilution was then  
666 volume normalized to obtain the final lentiviral titer.

667 To transduce hTERT–RPE1 cells, they were seeded at an appropriate density for each  
668 experiment with a maximal confluency of 60–70%. On the day of transduction, polybrene was  
669 added to the media to a final concentration of 8  $\mu$ g/ml. The volume of lentiviral supernatant was  
670 calculated on the basis of the diversity of the respective library and of the desired coverage and  
671 multiplicity of infection (MOI) of the experiment. A MOI of 0.5 was applied to all screens. The  
672 number of cells that were transduced at the beginning of an experiment was calculated by  
673 multiplying the diversity of the library with the desired coverage and needed MOI.

674

### 675 **3Cs CRISPR screening**

#### 676 *Library distribution and experimental coverage interdependency screening*

677 To explore the interdependency of multiplexed CRISPR library distribution and experimental  
678 screening coverage, three distorted 3Cs multiplex libraries were generated (see ‘generation of  
679 distorted libraries’) that represented libraries of different gRNA distributions. All three libraries  
680 were screened with a 20-fold and 200-fold coverage, each in triplicates. For the 20-fold screening,  
681 for each replicate, 1.1 million SpCas9 expressing hTERT–RPE1 cells were plated (0.37 million  
682 cells per flask) and transduced with the respective library with a MOI of 0.5. After 48 hrs the cells  
683 were selected with 2  $\mu$ M puromycin and kept in growing conditions for 14 days. At day 14, the  
684 cells were harvested, pooled and stored at -20°C until their genomic DNA was extracted and  
685 processed for NGS. For the 200-fold screening a total of 11 million (0.5 million cells per flask)  
686 SpCas9 expressing hTERT–RPE1 cells were plated and transduced with the respective library  
687 with a MOI of 0.5. Further screening was performed identically to the 20-fold screen.

688

#### 689 *Combinatorial 3Cs-gRNA autophagy screening*

690 Autophagy single and combinatorial gRNA screens for single or synergistic autophagy inhibition  
691 were performed in biological replicates and triplicates in the monoclonal hTERT–RPE1 cell line  
692 that stably expresses *Streptococcus pyogenes* Cas9 (SpCas9) and the autophagic flux probe  
693 (GFP-LC3-RFP)<sup>56</sup>, respectively. For each replicate 20 million cells (10 million for each, end time  
694 point and day 2 control) were transduced with lentiviral supernatant of the autophagy multiplex  
695 library with an MOI of 0.5 and a 1000- or 20-fold library coverage for single or combinatorial  
696 autophagy library screening, respectively. The control time points were harvested 2 days post-

697 transduction. All remaining cells were kept in growing conditions until day 7, at what point the cells  
698 were passaged, pooled and reseeded at library-diversity-maintaining density. After 13, 14 and 15  
699 days the cells were treated with the mTOR inhibitor Torin1 (250 nM, InvivoGen, 1222998-36-8)  
700 for 24 hrs in three batches to induce autophagy. After 24 hrs of Torin1 treatment, cells were  
701 collected and 50,000 to 100,000 cells for single or 1.5 to 2.25 million cells for combinatorial  
702 screening of each batch were FACS sorted to enrich for cells with blocked autophagy. The sorted  
703 cells were reseeded and expanded for seven days before they were harvested, pooled and stored  
704 at -20°C until their genomic DNA was extracted and processed for NGS.

705

## 706 **FACS**

707 Cell sorting was carried out with the FACS core facility of the Georg-Speyer Haus on a BD  
708 FACSAria Fusion, and CRISPR screening hit validation analysis on a FACSCanto II flow  
709 cytometer (BD Biosciences). Data was processed by FlowJo (FlowJo, LLC). Gating was carried  
710 out on the basis of viable and single cells that were identified on the basis of their scatter  
711 morphology.

712

## 713 **Arrayed autophagy candidate validation**

714 The validation of single and combinatorial autophagy screening hits was performed in arrayed  
715 conditions (one knockout per well). To do so, single and dual gene-targeting CRISPR constructs  
716 were designed and generated. For each gene, the top scoring guide sequence was selected with  
717 Azimuth 2.0 of the GPP sgRNA Designer ([https://portals.broadinstitute.org/gpp/public/analysis-  
718 tools/sgrna-design](https://portals.broadinstitute.org/gpp/public/analysis-tools/sgrna-design)) and purchased as forward and reverse oligonucleotide with compatible  
719 overhangs for restriction enzyme cloning (see 'DNA oligonucleotides'). The two oligonucleotides  
720 containing the gRNA target site were annealed and cloned into a restriction-enzyme digested and  
721 gel purified CRISPR vector. In more detail, single gRNA constructs were cloned into lenti-sgRNA  
722 blast vector (Addgene: 104993) by BsmBI restriction enzyme cloning. For combinatorial hit  
723 validation the dual CRISPR gRNA expression cassettes of pKLV2.2-h7SKgRNA5(SapI)-  
724 hU6gRNA5(BbsI)-PGKpuroBFP-W (Addgene: 72666) was cloned into the lenti-sgRNA blast  
725 plasmid to enable blasticidin selection of dual gRNA constructs. A silent point-mutation was  
726 introduced to remove the BbsI recognition site within the blasticidin sequence to allow the  
727 subsequent insertion of one gRNA by SapI (NEB, R0569) cloning into the h7SK expression  
728 cassette and the second gRNA by BbsI (NEB, R0539) cloning into the hU6 expression cassette.  
729 After cloning and sequence verification by SANGER sequencing, lentiviral supernatant was  
730 generated for each construct as described. Monoclonal hTERT-RPE1 cells with stable SpCas9

731 and GFP-LC3-RFP reporter expression were plated in 6-well plates with 50,000 cells per well.  
732 The following day, cells were transduced in the presence of 8 µg/ml polybrene (Sigma, H9268)  
733 with lentiviral supernatant. After 48 hrs the cells were selected with 10 µg/ml blasticidin  
734 (InvivoGen, ant-bl) for 7 days, passaged and cultivated at 40-60% confluency under constant  
735 blasticidin selection for an additional 7 days. At day 14, cells were treated with Torin1 to induce  
736 autophagy for 24 hrs until they were collected at day 15 and subject to FACS cell sorting to  
737 measure single or dual gene-knockout-induced autophagy blockage.

738

### 739 **gRNA performance and TIDE assay**

740 Guide RNA performance was evaluated by TIDE assay, as described previously<sup>45,71</sup>. In short, for  
741 each gRNA sequence, +/- 400 nucleotides from the gRNA annealing site, PCR primers were  
742 designed to result in a PCR product of 800 to 1000 nts in length. The gRNA-locus is then PCR  
743 amplified with OneTaq DNA polymerase (NEB, M0480) using 1 µg of genomic DNA, 40 µM dNTPs  
744 (final concentration), 0.2 µM of each forward and reverse amplification primer, 10x OneTaq  
745 standard buffer, and 2.5 units of OneTaq DNA polymerase. PCR cycles were set up as follows:  
746 initial denaturation at 94°C for 3 min, 39 cycles of denaturation at 94°C for 20 s, annealing at 55°C  
747 for 30 s, strand extension at 68°C for 2 min, and final strand extension at 68°C for 5 min. The  
748 PCR products were analyzed on a 0.8% TAE/agarose gel (100 V, 30 min) and purified using a  
749 Thermo Fisher Scientific GeneJET Gel Extraction Kit according to the manufacturer's protocol.  
750 The purified PCR product was pre-mixed with forward amplification primer and processed by  
751 SANGER sequencing, after which wildtype and gRNA-treated SANGER chromatograms were  
752 analyzed by TIDE and the percentage of unedited DNA extracted (<https://tide.deskgen.com/>).

753

### 754 **Data availability**

755 NGS data are provided as raw read count tables as Supplementary Table 4. Plasmids encoding  
756 for extended- and combinatorial-autophagy libraries will be available through the Goethe  
757 University Depository (<http://www.innovectis.de/INNOVECTIS-Frankfurt/Technologieangebote/Depository>).

759

### 760 **Code availability**

761 Custom software is publicly available from GitHub, <https://github.com/GEG-IBC2/3Cs-MPX>  
762 (GEG-IBC2, 2019; copy archived at <https://github.com/elifesciences-publications/3Cs>).

763

### 764 **DNA oligonucleotides and oligo pools**

765 Sequences of used DNA oligonucleotides and for 3Cs libraries are provided in Supplementary  
766 Table 2.

767

## 768 **FUNDING**

769 Hessisches Ministerium für Wissenschaft und Kunst (IIL5-518/17.004)

770 Hessisches Ministerium für Wissenschaft und Kunst (IIL5-519/03/03.001)

771 Deutsche Forschungsgemeinschaft (EXC115/2)

772 Deutsche Forschungsgemeinschaft (EXC147/2)

773 Deutsche Forschungsgemeinschaft (EXC 2026)

774

775 Funders had no role in study design, data collection and interpretation, or the decision to submit  
776 the work for publication.

777

## 778 **ACKNOWLEDGEMENTS**

779 We thank Andreas Ernst and Svenja Wiechmann for technical advice, Andrea Ballabio and  
780 Davide Cacchiarelli of the Telethon Institute of Genetics and Medicine, as well as Sebastian  
781 Wagner and Khalil Abou Elardat of the Cancer Genomics Core Facility Frankfurt, plus Tobias  
782 Schmidt of the Institute of Biochemistry I (Pathobiochemistry) for valuable support with NGS. This  
783 work was supported by the Hessian Ministry for Science and the Arts (HMWK, LOEWE-CGT,  
784 IIL5-518/17.004), the German Research Foundation (DFG; CEF-MC - EXC115/2; ECCPS -  
785 EXC147/2; CPI - EXC 2026) and in part by the LOEWE Center Frankfurt Cancer Institute (FCI)  
786 funded by the Hessen State Ministry for Higher Education, Research and the Arts (IIL5-  
787 519/03/03.001-0015).

788

## 789 **COMPETING INTERESTS**

790 The Goethe University Frankfurt has filed a patent application related to this work on which  
791 Valentina Diehl, Martin Wegner, Ivan Dikic and Manuel Kaulich are inventors (WO2017EP84625).  
792 The Goethe University provides an exclusive license of the 3Cs technology to Vivlion GmbH for  
793 which Ivan Dikic and Manuel Kaulich are co-founders, shareholders and chief officers.

794

## 795 **FIGURE LEGENDS**

796 **Figure 1. 3Cs multiplexing for combinatorial CRISPR gRNA libraries. A)** 3Cs  
797 multiplexing workflow. Two gRNA-encoding oligonucleotide pools are selectively



798 annealed to one of the gRNA-expression cassettes of the dU-containing ssDNA template  
799 plasmid for T7 DNA Pol-dependent generation of heteroduplex dU-dsDNA. Amplification  
800 in dut/ung-positive bacteria amplifies the combinatorial gRNA plasmid. See Material and  
801 Methods for a more details. **B)** Cas9 GFP/mCherry multiplex library design. Combinatorial  
802 gRNA constructs target GFP and mCherry genes simultaneously; each gene is  
803 individually targeted by 50 gRNAs, both genes are simultaneously targeted with 2601  
804 gRNA combinations. The single guide GFP-targeting library contains the wildtype gRNA  
805 placeholder in the hU6 cassette (mCherry), and vice versa. **C)** Gel-electrophoresis after  
806 analytical restriction enzyme digest of final 3Cs single and combinatorial libraries. **D)**  
807 Area-under-the-curve (AUC) determination of single and combinatorial library  
808 representation. As a reference, a perfectly distributed library (ideal) is shown in grey.  
809 Percentages indicate a library's representation at 90% of cumulative reads. AUC values  
810 are indicated next to each library's identifier. **E)** FACS analysis of GFP- and mCherry-  
811 positive hTERT-RPE1 cells after transduction with single or combinatorial libraries. Error  
812 bars represent standard deviations (SDs) over three biological replicates (n = 3).

813

814 **Figure 2. Library distribution skew dictates experimental scale and data quality. A)**  
815 Area-under-the-curve (AUC) determination of the nucleotide-randomized libraries. As a  
816 reference, a perfectly distributed library (ideal) is shown in grey. Percentages indicate  
817 library representations at 90% of cumulative reads. AUC values are indicated next to each  
818 library's identifier. **B)** Analysis of NHT-fraction in the biased 3Cs libraries. Median and  
819 quartiles of the distributions are shown as red straight and black dotted line, respectively.  
820 **C)** Area-under-the-curve (AUC) determination of the biased libraries. As a reference, a  
821 perfectly distributed library (ideal) is shown in grey. Percentages indicate a library's  
822 representation at 90% of cumulative reads. AUC values are indicated next to each  
823 library's identifier. **D)** Density plots showing the log<sub>2</sub>FC separation of combinatorial gRNA  
824 constructs targeting core essential genes (blue) and non-essential controls (green) in  
825 experimental coverages of 20x (dotted) and 200x (straight). QS: quality score. **E)** Analysis  
826 of the number of depleted gene-pairs detected with MAGeCK at the indicated FDR and  
827 log<sub>2</sub>FC cutoffs. **F)** Determination of the number of depleted gene-pairs at the indicated



828 FDR and log2FC cutoffs from sub-sampled read-count tables of replicates for each  
829 coverage containing 1 to 16 randomly chosen gRNA pairs.

830

831 **Figure 3. Single and multiplex-inherent single gRNA enrichment screens are**  
832 **complementary. A)** Cas9 autophagy single and multiplex library design. Combinatorial  
833 gRNA constructs target extended and core autophagy genes; each gene is targeted by 4  
834 gRNAs, 192 extended autophagy genes and 64 core autophagy genes with 10% of NHT  
835 controls per cassette generating 247,032 gRNA combinations. Single gRNA extended  
836 autophagy library contains the wildtype gRNA placeholder in the hU6 cassette (core  
837 autophagy). **B)** Single (s) and combinatorial (mpx) autophagy screening workflow. Cov.:  
838 coverage (library representation); MOI: multiplicity of infection; FACS: fluorescence-  
839 activated cell sorting; NGS: next-generation sequencing. **C)** Cell sorting representations  
840 of single and combinatorial (MPX) screen of post-FACS gate (#) and high-gate (\*). **D)**  
841 MAGeCK analysis of dedicated single gRNA autophagy screen of pre- and post-FACS  
842 samples with hit genes in red when matching cutoff criteria of  $FDR \leq 10\%$  and  $p$ -  
843 value  $\leq 0.05$ . Screen-selective hits in blue. **E)** MAGeCK analysis of multiplex-inherent  
844 single gRNA autophagy screen of pre- and post-FACS samples with hit genes in red when  
845 matching cutoff criteria of  $FDR \leq 10\%$  and  $p$ -value  $\leq 0.05$ . Screen-selective hits in blue. **F)**  
846 Analysis of single hit genes derived from D) and E) in arrayed autophagy blockage  
847 validations (red). Evaluation of gRNA activity by TIDE analysis (grey). Error bars  
848 represent standard error of mean (SEM) over three biological replicates per autophagy  
849 blockage (n=3). ND: not determined.

850

851 **Figure 4. Paralogs are redundant in autophagy. A)** MAGeCK analysis of combinatorial  
852 gRNAs targeting gene pairs in which both genes were identified as essential for  
853 autophagy of pre- and post-FACS samples. Hit gene pairs are shown in red when  
854 matching cutoff criteria of  $p$ -value  $\leq 0.05$ . **B)** MAGeCK analysis of combinatorial gRNAs  
855 targeting gene pairs in which one gene was identified as essential for autophagy of pre-  
856 and post-FACS samples. Hit gene pairs are shown in blue when matching cutoff criteria  
857 of  $p$ -value  $\leq 0.05$ . **C)** MAGeCK analysis of combinatorial gRNAs targeting gene pairs with  
858 neither gene being identified as essential for autophagy of pre- and post-FACS samples.

859 Hit gene pairs are shown in yellow when matching cutoff criteria of  $p\text{-value} \leq 0.05$ . Ras-  
860 related protein family (RAB) and ATG2 gene pairs are shown in blue and green,  
861 respectively. **D)** Global view on identified gene pairs per category in percent. Ess:  
862 essential; non-ess: non-essential. Color code adapted from A) to C). **E-G)** Arrayed  
863 analysis of hit gene pairs and the induced blockage of autophagy per gene knockout of  
864 each category, color code of A) to C). Control genes and sequences are shown in grey.  
865 Error bars represent standard error of mean (SEM) over three biological replicates ( $n=3$ ).  
866 **H)** Density plots of delta  $\log_2\text{FC}$  ( $\Delta\log_2\text{FC}$ ) analyses computed by MAX, SUM, MIN,  
867 MULT, and LOG models. **I)** Correlation between observed and expected  $\log_2\text{FC}$  values,  
868 derived from MAX model, for combinatorial gene-targeting. Data points above standard  
869 deviation and with  $p\text{-values} \leq 0.05$ , derived from C), are highlighted in yellow, representing  
870 synergistic gene interactions in autophagy. **J)** Network analysis of synergistic autophagy  
871 gene pairs, derived from I). Edge color and width set to  $\Delta\log_2\text{FC}$  values derived from  
872 MAX model. Edges and nodes of paralog gene pairs are highlighted in pink.

873

874 **Supp. Figure 1. A)** Analysis of single and multiplex dU-containing hetero-duplex 3Cs  
875 DNA by gel-electrophoresis. **B)** NGS sequencing depth of single and combinatorial GFP,  
876 mCherry, and GFP+mCherry 3Cs libraries. A sample's median and quartiles are shown  
877 as red straight and black dotted line, respectively. **C)** Analysis of distribution skew (skew)  
878 and completeness (compl.) per library, based on read counts derived from B).

879

880 **Supp. Figure 2. A)** NGS sequencing depth of nucleotide-randomized combinatorial 3Cs  
881 libraries (1-4N). A library's median and quartiles are shown as red straight and black  
882 dotted line, respectively. **B)** Analysis of distribution skew (skew) and completeness  
883 (compl.) per library, based on read counts derived from A). **C)** NGS sequencing depth of  
884 distribution skew biased combinatorial 3Cs libraries (1:1, 1:10, 1:100). A sample's median  
885 and quartiles are shown as red straight and black dotted line, respectively. **D)** Analysis of  
886 distribution skew (skew) and completeness (compl.) per library, based on read counts  
887 derived from C).

888

889 **Supp. Figure 3. A-B)** Pairwise sample correlation (Pearson's correlation coefficient),  
890 visualized as hierarchically clustered heatmaps (n), library distributions skews (1:1, 1:10,  
891 1:100) and coverages (20x, 200x) on gRNA-pair (A) and gene-pair (B) levels. Color code  
892 based on Pearson's correlation coefficient ( $\rho$ ) of normalized gRNA read counts.

893  
894 **Supp. Figure 4. A)** FACS analysis of monoclonal hTERT-RPE1 GFP-LC3B-RFP reporter  
895 cell line under conditions of basal autophagy (Basal), Torin1-induced autophagy  
896 (+Torin1), and Torin1-induced but Bafilomycin A1-blocked autophagy (+Torin1 +  
897 Bafilomycin A1). Gating is based on Torin1-induced reduction of GFP signal; percentage  
898 (%) of cells in gate. **B)** Analysis of NGS sequencing depth per 3Cs library (single, mpX)  
899 and replicate post-FACS sample (1-3). A sample's median and quartiles are shown as  
900 red straight and black dotted line, respectively. **C)** Analysis of distribution skew (skew)  
901 and completeness (compl.) per autophagy library (single, mpX), based on read counts  
902 derived from B). **D)** Area-under-the-curve (AUC) determination of the single and  
903 combinatorial (multiplex) autophagy libraries. As a reference, a perfectly distributed library  
904 (ideal) is shown in grey. AUC values are indicated next to each library's identifier.

905  
906 **Supp. Figure 5. A-D)** Pairwise sample correlation (Pearson's correlation coefficient),  
907 visualized as hierarchically clustered heatmaps (1-3) of pre- and post-FACS samples of  
908 autophagy enrichment screens with single (B) and combinatorial gRNA-targeting in  
909 autophagy blockage (C) and high-gates (D) on gRNA and gene level. Color code based  
910 on Pearson's correlation coefficient ( $\rho$ ) of normalized gRNA read counts. **E)** Analysis of  
911 ATG4B-associated guide pairs in high-gate post-FACS samples.

912  
913 **Supp. Figure 6. A-B)** MAGeCK analysis of dedicated single (A) and multiplex-inherent  
914 single (B) gRNA autophagy screens between pre- and post-FACS samples with genes in  
915 red when matching cutoff criteria of  $p\text{-value} \leq 0.05$ . Screen-selective hits in blue.

916  
917 **Supp. Figure 7. A)** Log<sub>2</sub>FC-analysis of targeting a single gene with one (single) or two  
918 (double) gRNAs. The dotted diagonal line represents equal phenotypic strength, based  
919 on FACS enrichment. **B)** Arrayed analysis of phenotypic strength of single essential

920 genes for autophagy when targeted with one (yellow) or two (blue) gRNAs. Error bars  
921 represent standard error of mean (SEM) over three biological replicates (n=3). **C**) Density  
922 plots of delta log<sub>2</sub>FC ( $\Delta\log_2\text{FC}$ ) value analyses of single essential genes for autophagy,  
923 computed by MAX, SUM, MIN, MULT, and LOG models.

924

## 925 REFERENCES

- 926 1. Maddalo, D. *et al.* In vivo engineering of oncogenic chromosomal rearrangements with  
927 the CRISPR/Cas9 system. *Nature* **516**, 423–428 (2014).
- 928 2. Cong, L. *et al.* Multiplex genome engineering using CRISPR/Cas systems. *Science* (80-  
929 ). **339**, 819–823 (2013).
- 930 3. Wong, A. S. L. *et al.* Multiplexed barcoded CRISPR-Cas9 screening enabled by  
931 CombiGEM. *Proc. Natl. Acad. Sci. U. S. A.* **113**, 2544–2549 (2016).
- 932 4. Tzelepis, K. *et al.* A CRISPR Dropout Screen Identifies Genetic Vulnerabilities and  
933 Therapeutic Targets in Acute Myeloid Leukemia. *Cell Rep* **17**, 1193–1205 (2016).
- 934 5. Kabadi, A. M., Ousterout, D. G., Hilton, I. B. & Gersbach, C. A. Multiplex CRISPR/Cas9-  
935 based genome engineering from a single lentiviral vector. *Nucleic Acids Res.* **42**, e147–  
936 e147 (2014).
- 937 6. Sakuma, T., Nishikawa, A., Kume, S., Chayama, K. & Yamamoto, T. Multiplex genome  
938 engineering in human cells using all-in-one CRISPR/Cas9 vector system. *Sci Rep* **4**,  
939 5400 (2014).
- 940 7. Vad-Nielsen, J., Lin, L., Bolund, L., Nielsen, A. L. & Luo, Y. Golden Gate Assembly of  
941 CRISPR gRNA expression array for simultaneously targeting multiple genes. *Cell. Mol.*  
942 *Life Sci.* **73**, 4315–4325 (2016).
- 943 8. Zuckermann, M. *et al.* A novel cloning strategy for one-step assembly of multiplex  
944 CRISPR vectors. *Sci. Rep.* **8**, (2018).
- 945 9. Albers, J. *et al.* A versatile modular vector system for rapid combinatorial mammalian  
946 genetics. *J. Clin. Invest.* **125**, 1603–1619 (2015).
- 947 10. Haldeman, J. M. *et al.* Creation of versatile cloning platforms for transgene expression  
948 and dCas9-based epigenome editing. *Nucleic Acids Res.* **47**, e23–e23 (2018).
- 949 11. Breunig, C. T. *et al.* One step generation of customizable gRNA vectors for multiplex  
950 CRISPR approaches through string assembly gRNA cloning (STAgR). *PLoS One* **13**,  
951 (2018).
- 952 12. Nissim, L., Perli, S. D., Fridkin, A., Perez-Pinera, P. & Lu, T. K. Multiplexed and

- 953 Programmable Regulation of Gene Networks with an Integrated RNA and CRISPR/Cas  
954 Toolkit in Human Cells. *Mol. Cell* **54**, 698–710 (2014).
- 955 13. Minkenberg, B., Wheatley, M. & Yang, Y. Chapter Seven - CRISPR/Cas9-Enabled  
956 Multiplex Genome Editing and Its Application. in *Gene Editing in Plants* (eds. Weeks, D.  
957 P. & Yang, B. B. T.-P. in M. B. and T. S.) **149**, 111–132 (Academic Press, 2017).
- 958 14. Vidigal, J. A. & Ventura, A. Rapid and efficient one-step generation of paired gRNA  
959 CRISPR-Cas9 libraries. *Nat Commun* **6**, 8083 (2015).
- 960 15. Shen, J. P. *et al.* Combinatorial CRISPR-Cas9 screens for de novo mapping of genetic  
961 interactions. *Nat. Methods* **14**, 573–576 (2017).
- 962 16. Han, K. *et al.* Synergistic drug combinations for cancer identified in a CRISPR screen for  
963 pairwise genetic interactions. *Nat. Biotechnol.* **35**, 463–474 (2017).
- 964 17. Mani, R., St Onge, R. P., Hartman, J. L., Giaever, G. & Roth, F. P. Defining genetic  
965 interaction. *Proc. Natl. Acad. Sci. U. S. A.* **105**, 3461–6 (2008).
- 966 18. Nijman, S. M. B. Synthetic lethality: General principles, utility and detection using genetic  
967 screens in human cells. *FEBS Letters* **585**, 1–6 (2011).
- 968 19. Chan, D. A. & Giaccia, A. J. Harnessing synthetic lethal interactions in anticancer drug  
969 discovery. *Nature Reviews Drug Discovery* **10**, 351–364 (2011).
- 970 20. Ramkumar, P., Kampmann, M. & Qian, C. CRISPR-based genetic interaction maps  
971 inform therapeutic strategies in cancer. *Translational Cancer Research* **7**, S61–S67  
972 (2018).
- 973 21. Ashworth, A. A Synthetic Lethal Therapeutic Approach: Poly(ADP) Ribose Polymerase  
974 Inhibitors for the Treatment of Cancers Deficient in DNA Double-Strand Break Repair. *J.*  
975 *Clin. Oncol.* **26**, 3785–3790 (2008).
- 976 22. Helleday, T. The underlying mechanism for the PARP and BRCA synthetic lethality:  
977 Clearing up the misunderstandings. *Molecular Oncology* **5**, 387–393 (2011).
- 978 23. Cho, S. Y. *et al.* A novel combination treatment targeting BCL-XL and MCL1 for  
979 KRAS/BRAF-mutated and BCL2L1-amplified colorectal cancers. *Mol. Cancer Ther.* **16**,  
980 2178–2190 (2017).
- 981 24. Najm, F. J. *et al.* Orthologous CRISPR–Cas9 enzymes for combinatorial genetic screens.  
982 *Nat. Biotechnol.* **36**, 179–189 (2017).
- 983 25. Mereniuk, T. R. *et al.* Synthetic lethal targeting of PTEN-deficient cancer cells using  
984 selective disruption of polynucleotide kinase/phosphatase. *Mol. Cancer Ther.* **12**, 2135–  
985 2144 (2013).
- 986 26. Neshat, M. S. *et al.* Enhanced sensitivity of PTEN-deficient tumors to inhibition of

- 987 FRAP/mTOR. *Proc. Natl. Acad. Sci. U. S. A.* **98**, 10314–10319 (2001).
- 988 27. Zamanighomi, M. *et al.* GEMINI: a variational Bayesian approach to identify genetic  
989 interactions from combinatorial CRISPR screens. *Genome Biol.* **20**, 137 (2019).
- 990 28. Klionsky, D. J. & Emr, S. D. Autophagy as a regulated pathway of cellular degradation.  
991 *Science* **290**, 1717–1721 (2000).
- 992 29. Dikic, I. & Elazar, Z. Mechanism and medical implications of mammalian autophagy.  
993 *Nature Reviews Molecular Cell Biology* **19**, 349–364 (2018).
- 994 30. Mizushima, N., Yoshimori, T. & Levine, B. Methods in Mammalian Autophagy Research.  
995 *Cell* **140**, 313–326 (2010).
- 996 31. Yoshii, S. R. & Mizushima, N. Monitoring and measuring autophagy. *International Journal*  
997 *of Molecular Sciences* **18**, (2017).
- 998 32. Morita, K. *et al.* Genome-wide CRISPR screen identifies TMEM41B as a gene required  
999 for autophagosome formation. *J Cell Biol* **217**, 3817–3828 (2018).
- 1000 33. Shoemaker, C. J. *et al.* CRISPR screening using an expanded toolkit of autophagy  
1001 reporters identifies TMEM41B as a novel autophagy factor. *PLoS Biol.* **17**, e2007044  
1002 (2019).
- 1003 34. Moretti, F. *et al.* TMEM 41B is a novel regulator of autophagy and lipid mobilization.  
1004 *EMBO Rep.* **19**, (2018).
- 1005 35. Jia, R. & Bonifacino, J. S. Negative Regulation of Autophagy by UBA6-BIRC6–Mediated  
1006 Ubiquitination of LC3. *bioRxiv* **8**, 699124 (2019).
- 1007 36. Orvedahl, A. *et al.* Autophagy genes in myeloid cells counteract IFN $\gamma$ -induced TNF-  
1008 mediated cell death and fatal TNF-induced shock. *Proc. Natl. Acad. Sci. U. S. A.* **116**,  
1009 16497–16506 (2019).
- 1010 37. Kerins, M. J. *et al.* Genome-Wide CRISPR Screen Reveals Autophagy Disruption as the  
1011 Convergence Mechanism That Regulates the NRF2 Transcription Factor. *Mol. Cell. Biol.*  
1012 **39**, (2019).
- 1013 38. Towers, C. G. *et al.* Cancer Cells Upregulate NRF2 Signaling to Adapt to Autophagy  
1014 Inhibition. *Dev. Cell* **50**, 690-703.e6 (2019).
- 1015 39. Potting, C. *et al.* Genome-wide CRISPR screen for PARKIN regulators reveals  
1016 transcriptional repression as a determinant of mitophagy. *Proc. Natl. Acad. Sci.* **115**,  
1017 201711023 (2017).
- 1018 40. Hoshino, A. *et al.* The ADP/ATP translocase drives mitophagy independent of nucleotide  
1019 exchange. *Nature* **575**, 375–379 (2019).
- 1020 41. Heo, J. M. *et al.* Integrated proteogenetic analysis reveals the landscape of a



- 1021 mitochondrial-autophagosome synapse during PARK2-dependent mitophagy. *Sci. Adv.* **5**,  
1022 (2019).
- 1023 42. Towers, C. G. & Thorburn, A. Therapeutic Targeting of Autophagy. *EBioMedicine* **14**, 15–  
1024 23 (2016).
- 1025 43. Levy, J. M. M., Towers, C. G. & Thorburn, A. Targeting autophagy in cancer. *Nature*  
1026 *Reviews Cancer* **17**, 528–542 (2017).
- 1027 44. Galluzzi, L., Bravo-San Pedro, J. M., Levine, B., Green, D. R. & Kroemer, G.  
1028 Pharmacological modulation of autophagy: Therapeutic potential and persisting  
1029 obstacles. *Nature Reviews Drug Discovery* **16**, 487–511 (2017).
- 1030 45. Wegner, M. *et al.* Circular synthesized CRISPR/Cas gRNAs for functional interrogations  
1031 in the coding and noncoding genome. *Elife* **8**, (2019).
- 1032 46. Dang, Y. *et al.* Optimizing sgRNA structure to improve CRISPR-Cas9 knockout efficiency.  
1033 *Genome Biol.* **16**, 280 (2015).
- 1034 47. Cross, B. C. S. *et al.* Increasing the performance of pooled CRISPR-Cas9 drop-out  
1035 screening. *Sci. Rep.* **6**, 1–8 (2016).
- 1036 48. Huang, R., Fang, P. & Kay, B. K. Improvements to the Kunkel mutagenesis protocol for  
1037 constructing primary and secondary phage-display libraries. *Methods* **58**, 10–17 (2012).
- 1038 49. Imkeller, K., Ambrosi, G., Boutros, M. & Huber, W. Gscreen: Modelling asymmetric  
1039 count ratios in CRISPR screens to decrease experiment size and improve phenotype  
1040 detection. *Genome Biol.* **21**, 53 (2020).
- 1041 50. Hart, T. *et al.* High-Resolution CRISPR Screens Reveal Fitness Genes and Genotype-  
1042 Specific Cancer Liabilities. *Cell* **163**, 1515–1526 (2015).
- 1043 51. Doench, J. G. *et al.* Optimized sgRNA design to maximize activity and minimize off-target  
1044 effects of CRISPR-Cas9. *Nat Biotechnol* **34**, 184–191 (2016).
- 1045 52. Kim, E. & Hart, T. Improved analysis of CRISPR fitness screens and reduced off-target  
1046 effects with the BAGEL2 gene essentiality classifier. *bioRxiv* 2020.05.30.125526 (2020).  
1047 doi:10.1101/2020.05.30.125526
- 1048 53. Li, W. *et al.* MAGeCK enables robust identification of essential genes from genome-scale  
1049 CRISPR/Cas9 knockout screens. *Genome Biol.* **15**, 554 (2014).
- 1050 54. Gonatopoulos-Pournatzis, T. *et al.* Genetic interaction mapping and exon-resolution  
1051 functional genomics with a hybrid Cas9–Cas12a platform. *Nat. Biotechnol.* **38**, 638–648  
1052 (2020).
- 1053 55. Ong, S. H., Li, Y., Koike-Yusa, H. & Yusa, K. Optimised metrics for CRISPR-KO screens  
1054 with second-generation gRNA libraries. *Sci. Rep.* **7**, 7384 (2017).



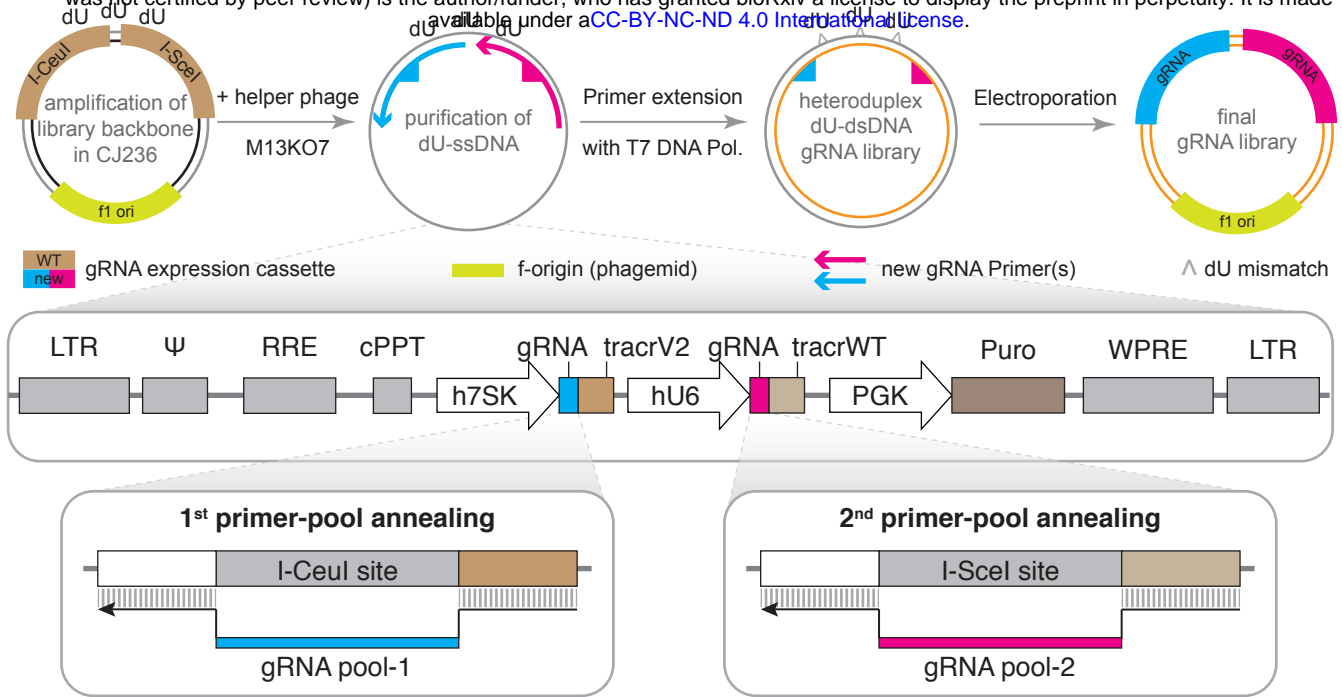
- 1055 56. Kaizuka, T. *et al.* An Autophagic Flux Probe that Releases an Internal Control. *Mol. Cell*  
1056 **64**, 835–849 (2016).
- 1057 57. Dejesus, R. *et al.* Functional CRISPR screening identifies the ufmylation pathway as a  
1058 regulator of SQSTM1/p62. *Elife* **5**, (2016).
- 1059 58. Goodwin, J. M. *et al.* Autophagy-Independent Lysosomal Targeting Regulated by  
1060 ULK1/2-FIP200 and ATG9. *Cell Rep.* **20**, 2341–2356 (2017).
- 1061 59. Peets, E. M. *et al.* Minimized double guide RNA libraries enable scale-limited  
1062 CRISPR/Cas9 screens. *bioRxiv* 859652 (2019). doi:10.1101/859652
- 1063 60. Costanzo, M. *et al.* A global genetic interaction network maps a wiring diagram of cellular  
1064 function. *Science* **353**, aaf1420 (2016).
- 1065 61. Xie, X., Le, L., Fan, Y., Lv, L. & Zhang, J. Autophagy is induced through the ROS-TP53-  
1066 DRAM1 pathway in response to mitochondrial protein synthesis inhibition. *Autophagy* **8**,  
1067 1071–1084 (2012).
- 1068 62. Gonçalves, E. *et al.* Minimal genome-wide human CRISPR-Cas9 library. *bioRxiv* 848895  
1069 (2019). doi:10.1101/848895
- 1070 63. Dede, M., McLaughlin, M., Kim, E. & Hart, T. Multiplex enCas12a screens show  
1071 functional buffering by paralogs is systematically absent from genome-wide  
1072 CRISPR/Cas9 knockout screens. *bioRxiv* 2020.05.18.102764 (2020).  
1073 doi:10.1101/2020.05.18.102764
- 1074 64. Folkerts, H. *et al.* Inhibition of autophagy as a treatment strategy for p53 wild-type acute  
1075 myeloid leukemia. *Cell Death Dis.* **8**, e2927 (2017).
- 1076 65. Rogov, V., Dötsch, V., Johansen, T. & Kirkin, V. Interactions between Autophagy  
1077 Receptors and Ubiquitin-like Proteins Form the Molecular Basis for Selective Autophagy.  
1078 *Molecular Cell* **53**, 167–178 (2014).
- 1079 66. Chen, B. *et al.* Dynamic imaging of genomic loci in living human cells by an optimized  
1080 CRISPR/Cas system. *Cell* **155**, 1479–1491 (2013).
- 1081 67. Martin, M. Cutadapt removes adapter sequences from high-throughput sequencing  
1082 reads. *EMBnet.journal* **17**, 10 (2011).
- 1083 68. Langmead, B. & Salzberg, S. L. Fast gapped-read alignment with Bowtie 2. *Nat. Methods*  
1084 **9**, 357–359 (2012).
- 1085 69. Waskom, M. *et al.* mwaskom/seaborn: v0.10.1 (April 2020). (2020).  
1086 doi:10.5281/ZENODO.3767070
- 1087 70. Shannon, P. *et al.* Cytoscape: A software Environment for integrated models of  
1088 biomolecular interaction networks. *Genome Res.* **13**, 2498–2504 (2003).

- 1089 71. Brinkman, E. K., Chen, T., Amendola, M. & van Steensel, B. Easy quantitative  
1090 assessment of genome editing by sequence trace decomposition. *Nucleic Acids Res* **42**,  
1091 e168 (2014).  
1092

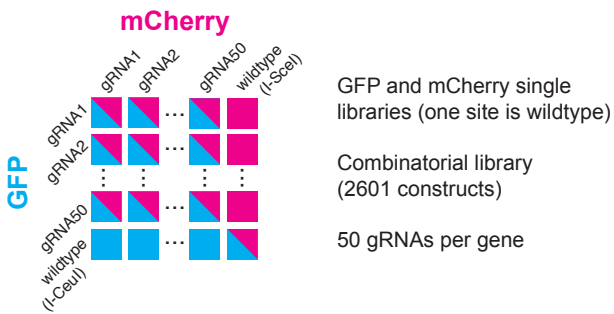
# Figure 1

**A**

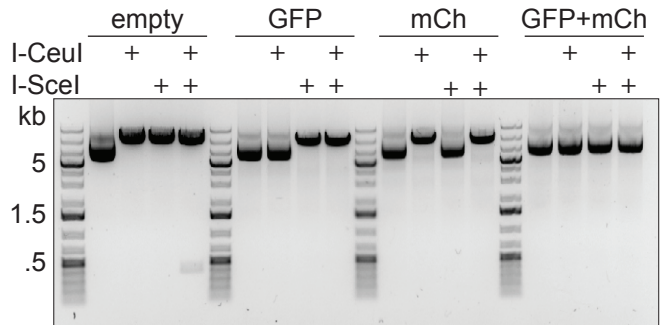
bioRxiv preprint doi: <https://doi.org/10.1101/2020.07.28.201152>; this version posted July 28, 2020. The copyright holder for this preprint (which was not certified by peer review) is the author/funder, who has granted bioRxiv a license to display the preprint in perpetuity. It is made available under aCC-BY-NC-ND 4.0 International license.



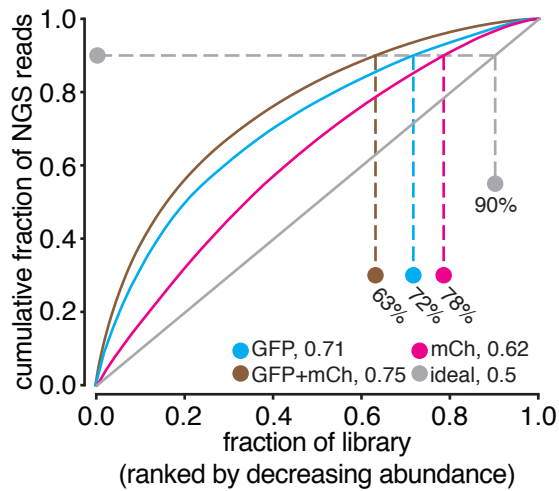
**B**



**C**



**D**



**E**

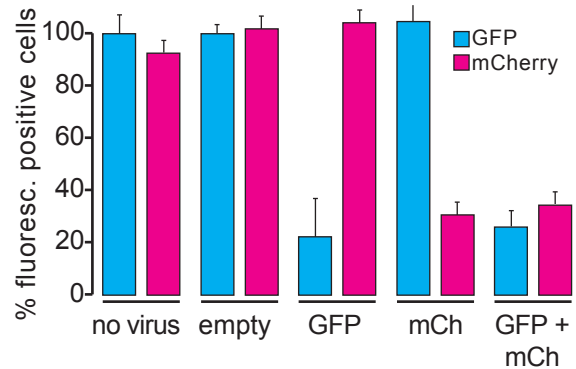


# Figure 2

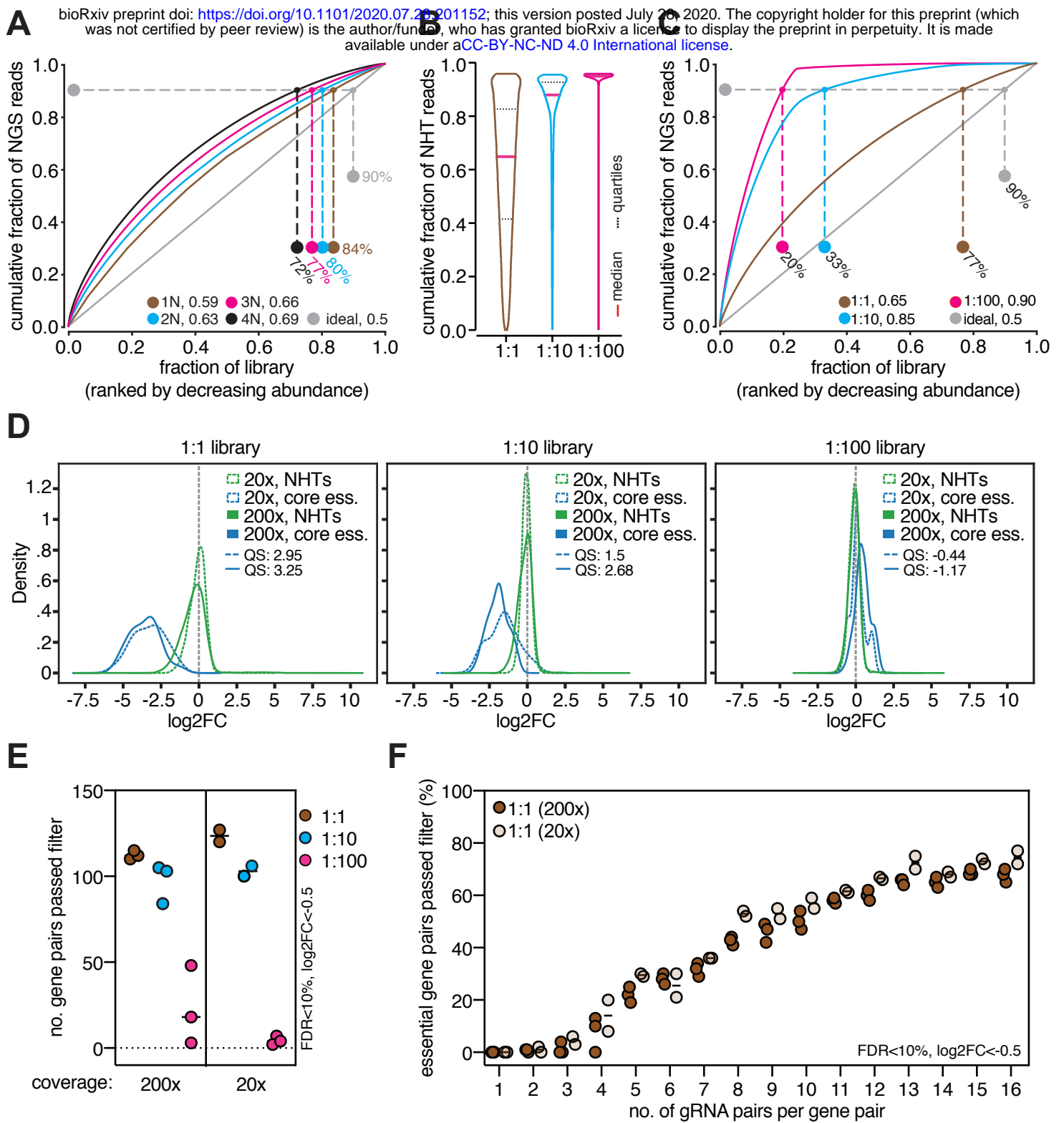


# Figure 3

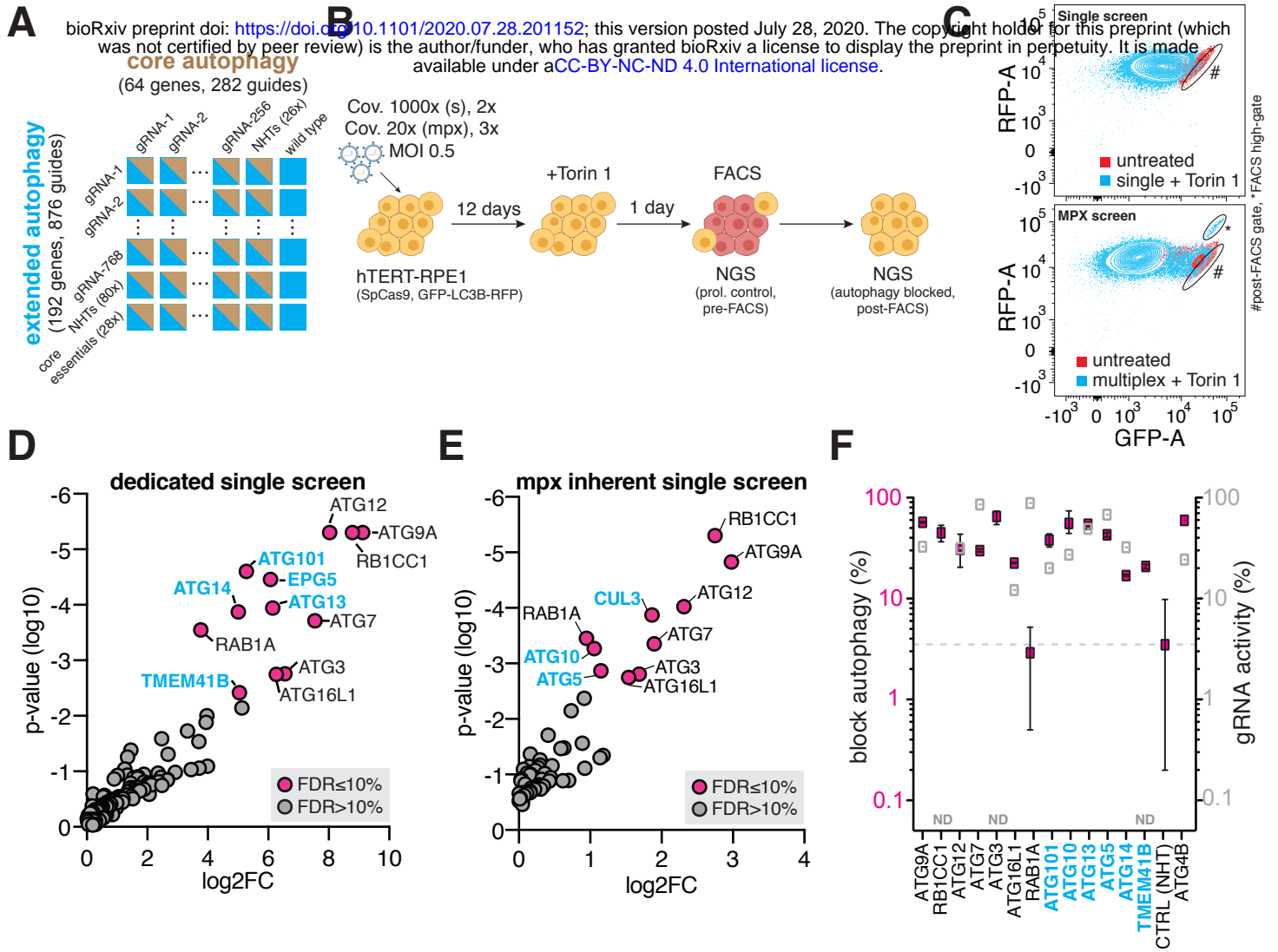
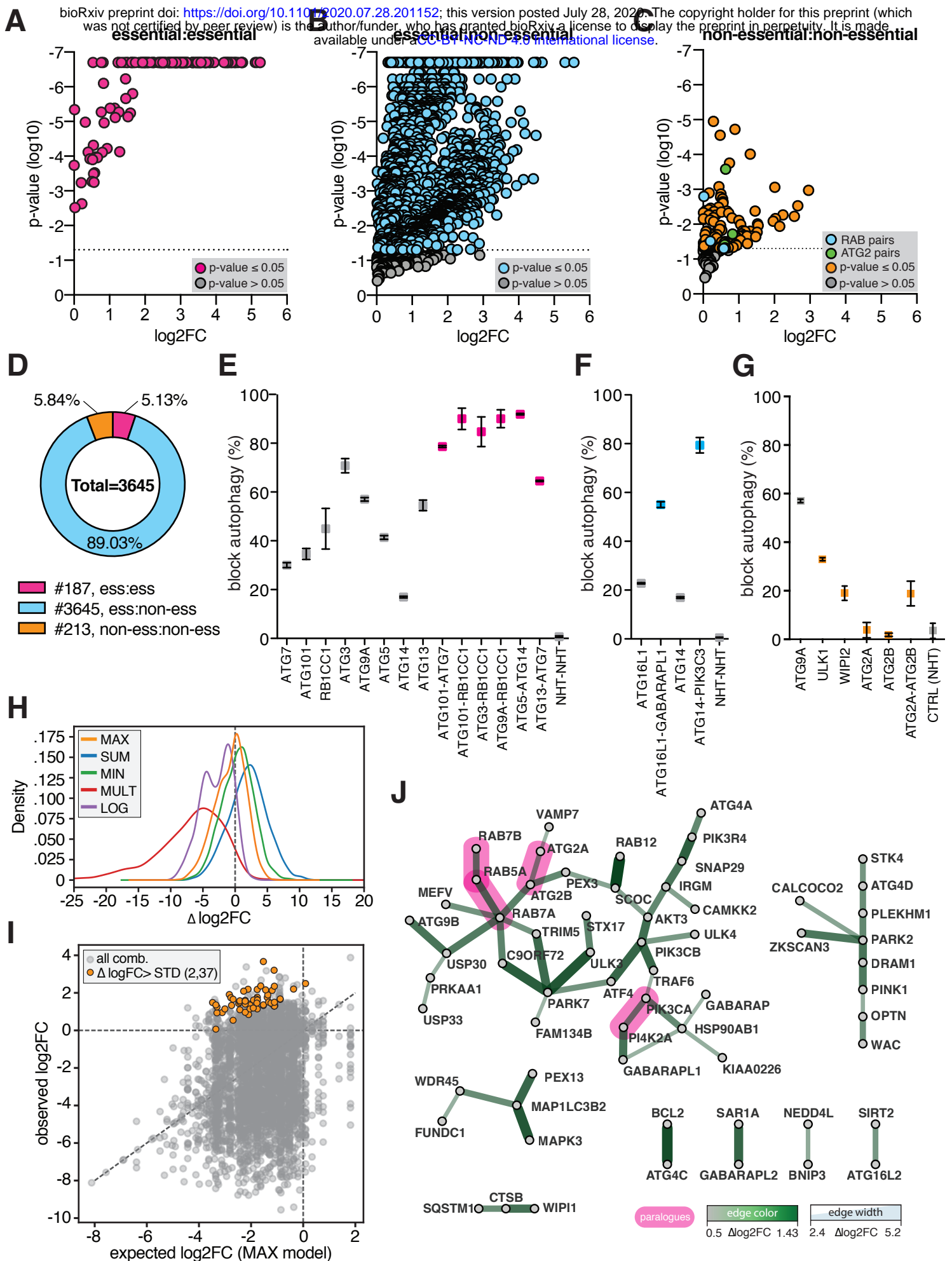


# Figure 4

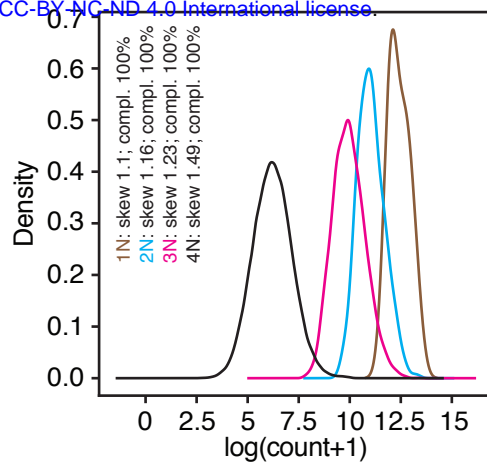
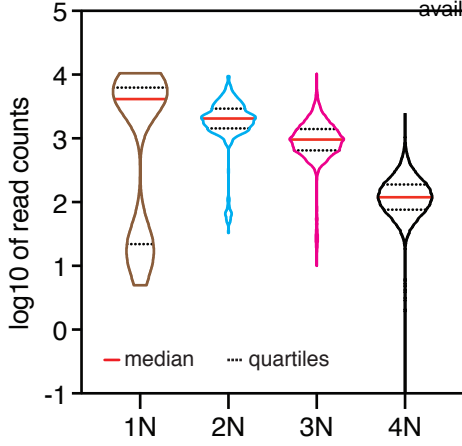




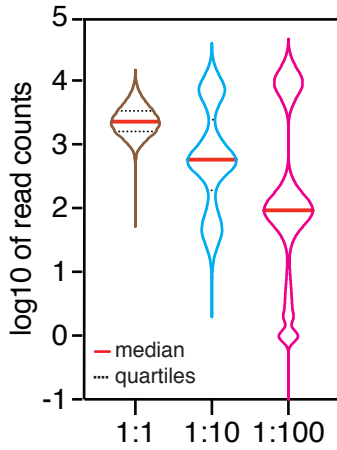


# Supp. Figure 2

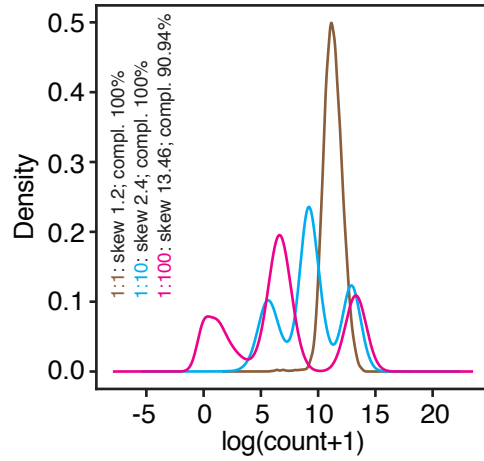
**A** bioRxiv preprint doi: <https://doi.org/10.1101/2020.07.28.234152>; this version posted July 28, 2020. The copyright holder for this preprint (which was not certified by peer review) is the author/funder, who has granted bioRxiv a license to display the preprint in perpetuity. It is made available under aCC-BY-NC-ND 4.0 International license.



**C**

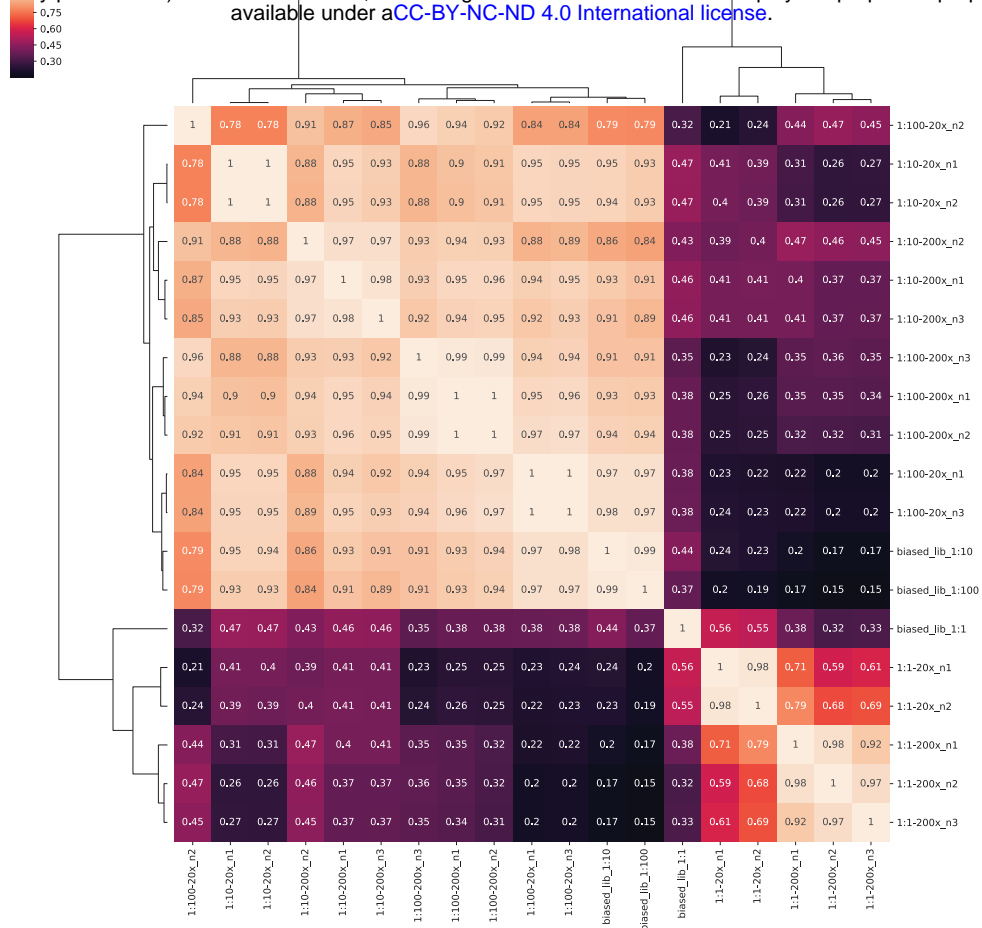


**D**

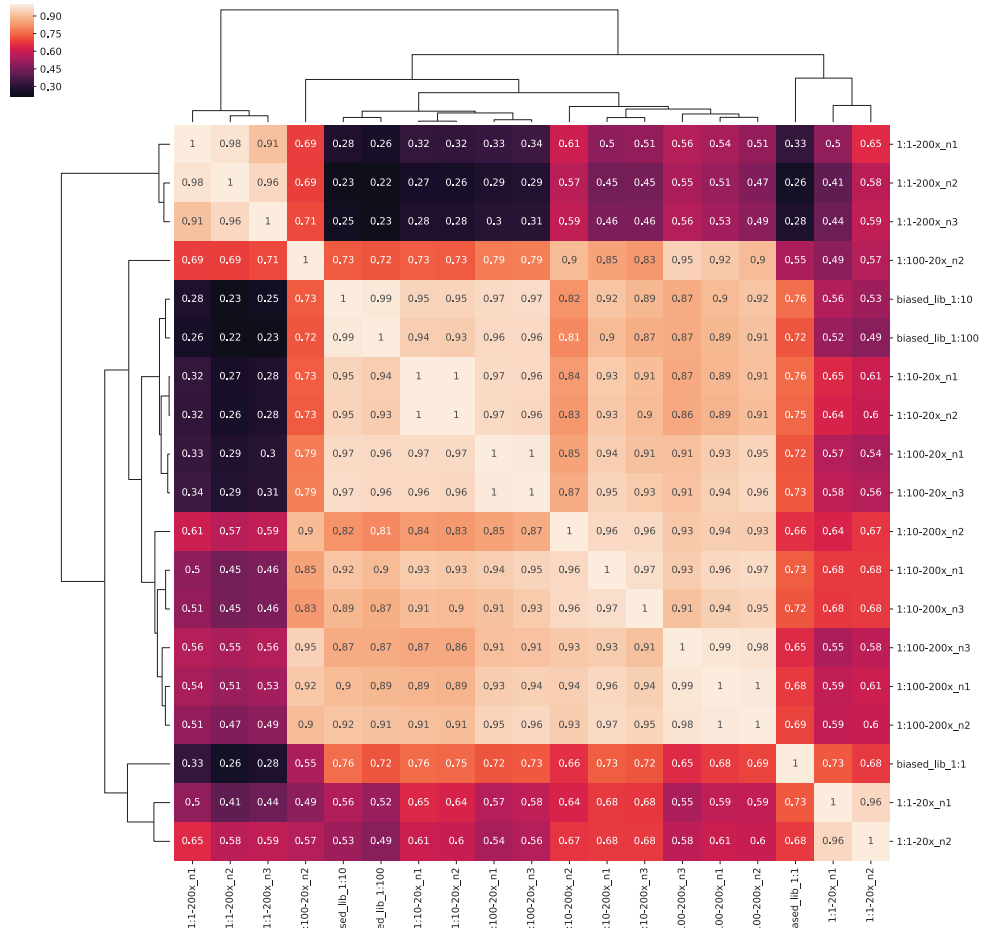


# Supp. Figure 3

**A** bioRxiv preprint doi: <https://doi.org/10.1101/2020.07.28.201152>; this version posted July 28, 2020. The copyright holder for this preprint (which was not certified by peer review) is the author/funder, who has granted bioRxiv a license to display the preprint in perpetuity. It is made available under a [CC-BY-NC-ND 4.0 International license](https://creativecommons.org/licenses/by-nc-nd/4.0/).



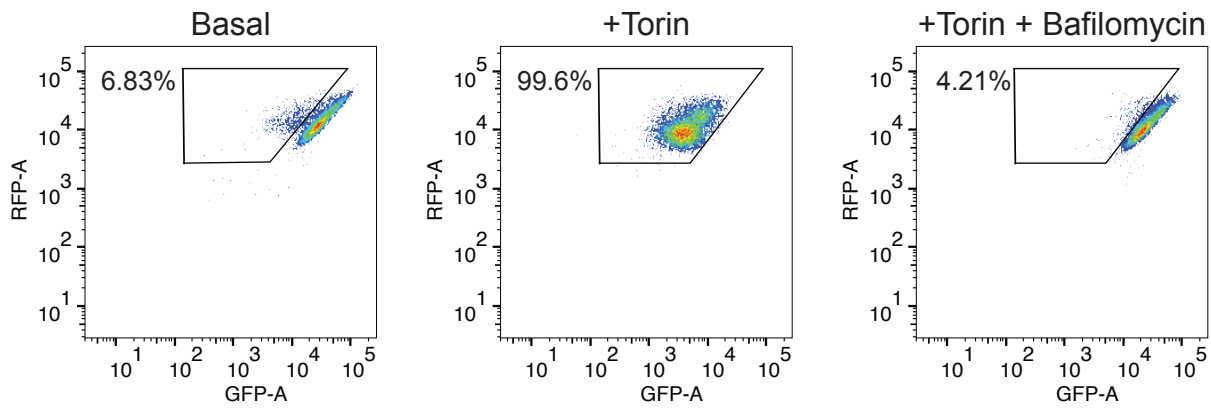
**B**



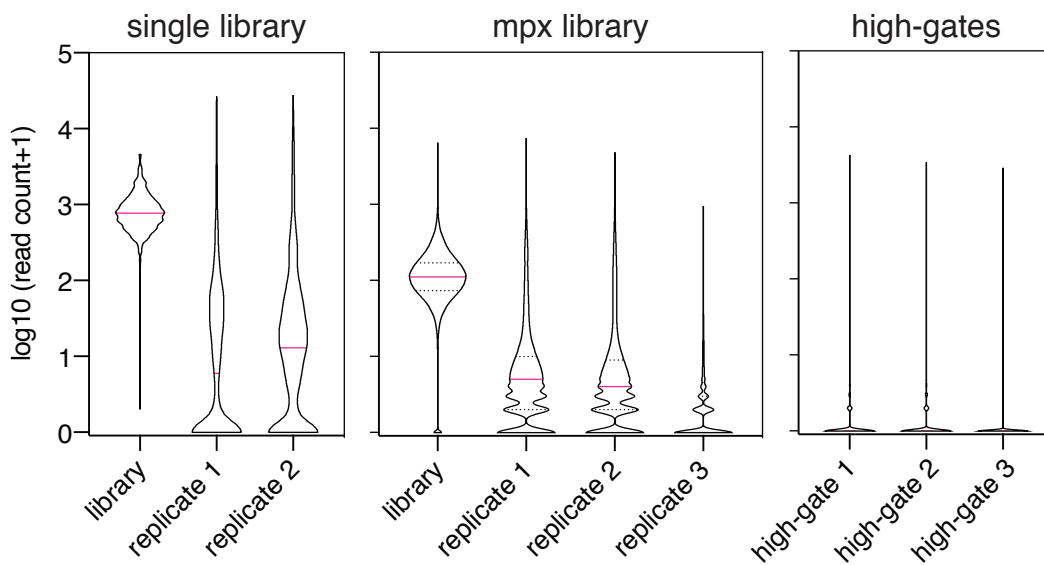
# Supp. Figure 4

bioRxiv preprint doi: <https://doi.org/10.1101/2020.07.28.201152>; this version posted July 28, 2020. The copyright holder for this preprint (which was not certified by peer review) is the author/funder, who has granted bioRxiv a license to display the preprint in perpetuity. It is made available under a [CC-BY-NC-ND 4.0 International license](#).

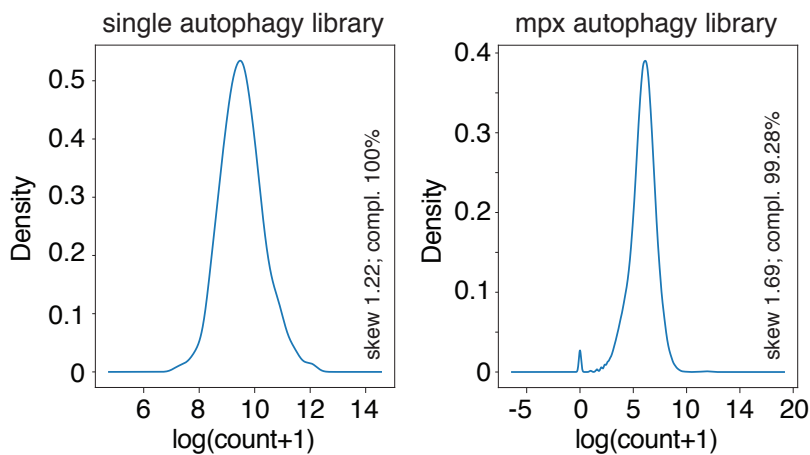
**A**



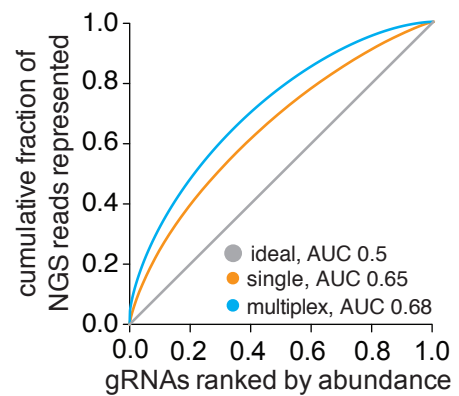
**B**



**C**

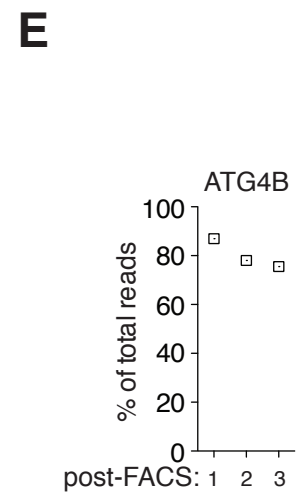
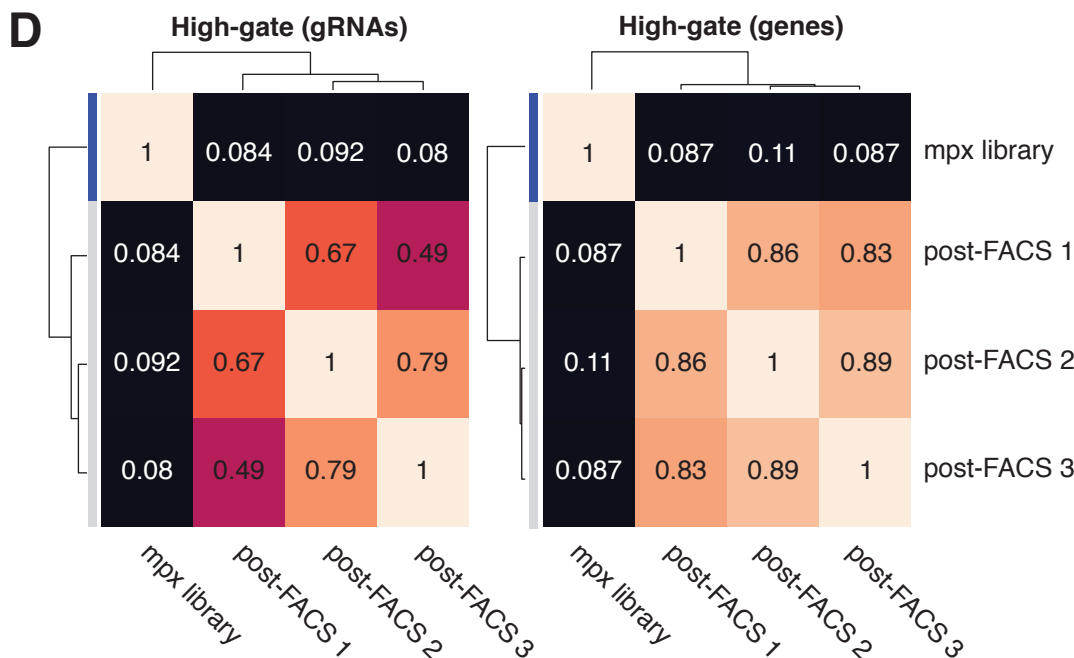
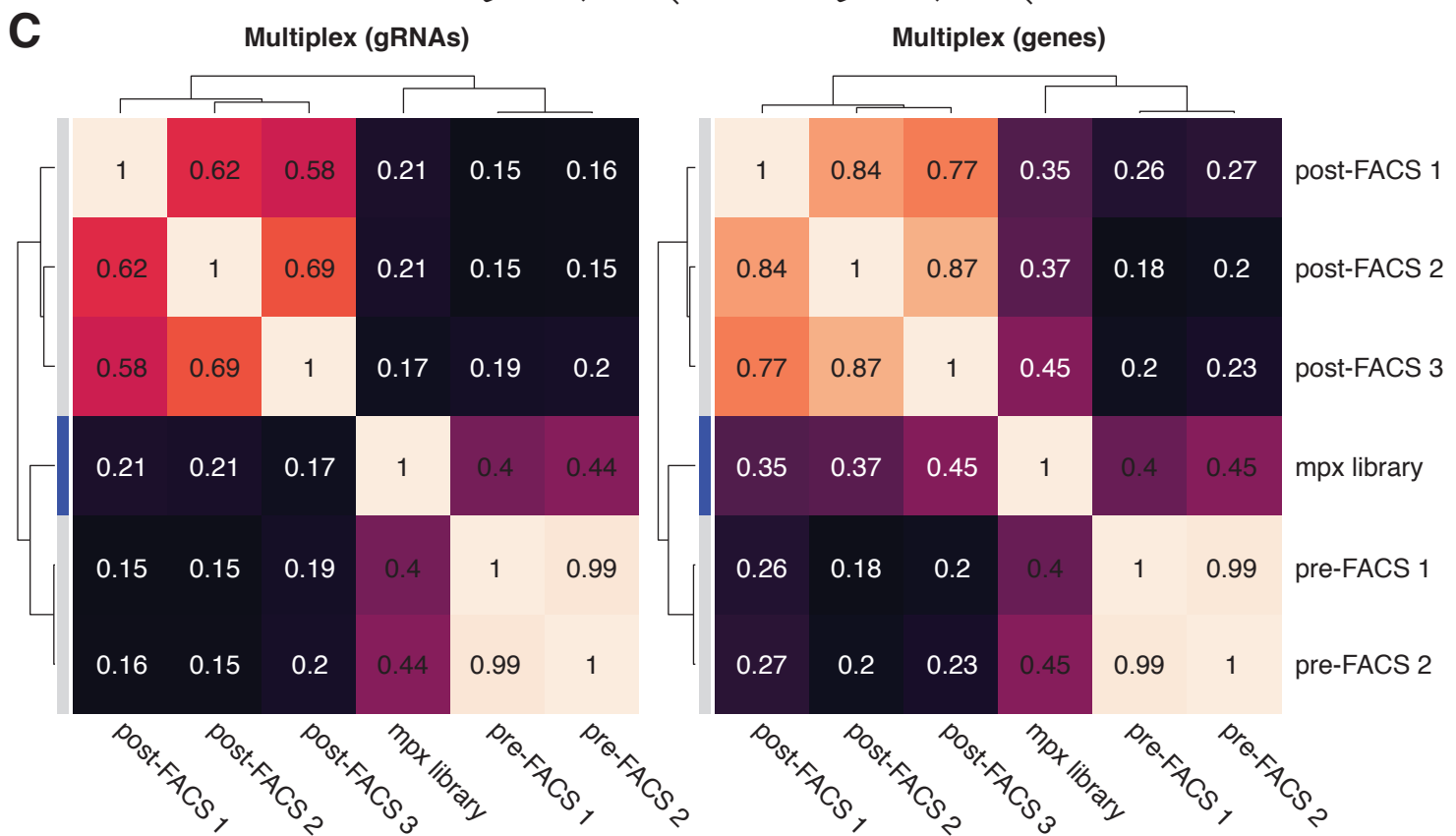
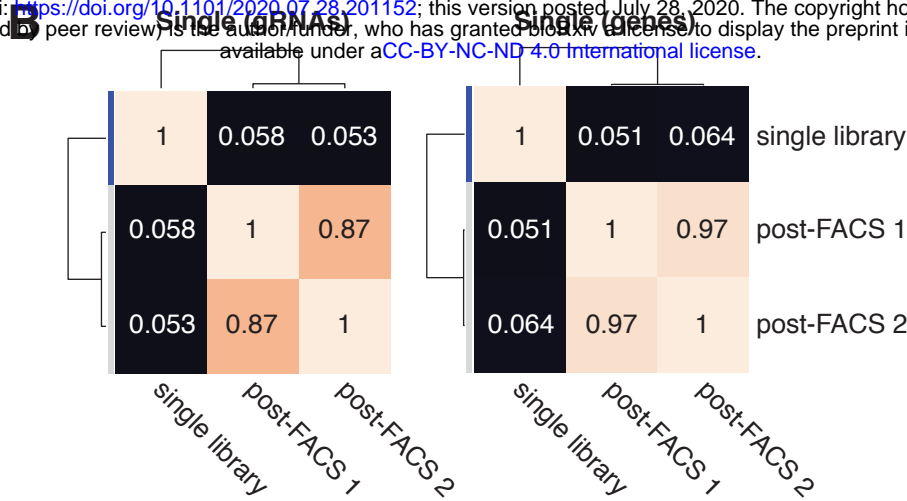
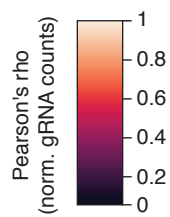


**D**



# Supp. Figure 5

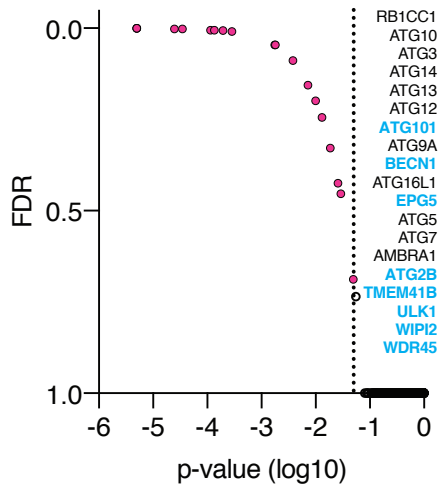
**A** bioRxiv preprint doi: <https://doi.org/10.1101/2020.07.28.201152>; this version posted July 28, 2020. The copyright holder for this preprint (which was not certified by peer review) is the author/funder, who has granted bioRxiv a license to display the preprint in perpetuity. It is made available under a [CC-BY-NC-ND 4.0 International license](https://creativecommons.org/licenses/by-nc-nd/4.0/).



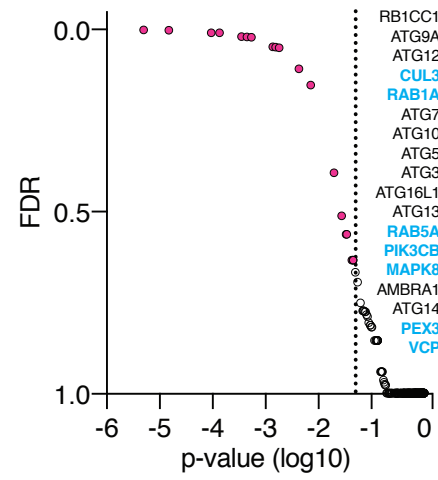
# Supp. Figure 6

**A** bioRxiv preprint doi: <https://doi.org/10.1101/2020.07.28.201152>; this version posted July 28, 2020. The copyright holder for this preprint (which was not certified by peer review) is the author/funder, who has granted bioRxiv a license to display the preprint in perpetuity. It is made available under a [CC-BY-NC-ND 4.0 International license](#).

**dedicated single screen**



**B** mpX inherent single screen





# Supp. Figure 7

**A** bioRxiv preprint doi: <https://doi.org/10.1101/2020.07.28.201152>; this version posted July 28, 2020. The copyright holder for this preprint (which was not certified by peer review) is the author/funder, who has granted bioRxiv a license to display the preprint in perpetuity. It is made available under aCC-BY-NC-ND 4.0 International license.

